Geoscience Frontiers 10 (2019) 2203–2218

HOSTED BY

Contents lists available at ScienceDirect

China University of Geosciences (Beijing)

Geoscience Frontiers

journal homepage: www.elsevier.com/locate/gsf

Research Paper

Testing carbonate chemostratigraphy across differentiated ancient shallow-platform environments (Early Kimmeridgian, S Iberia)

Rute Coimbra [a,b,*], Beatriz Marques [c], Federico Olóriz [d]

[a] GeoBioTec, Departamento de Geociências, Universidade de Aveiro, Portugal
[b] MARE, Departamento de Ciências da Terra, Universidade de Coimbra, Portugal
[c] Faculdade de Ciências e Tecnologia, Universidade Nova de Lisboa, Portugal
[d] Departamento de Estratigrafia y Palaeontologia, Universidad de Granada, Spain

ARTICLE INFO

Article history:
Received 11 June 2018
Received in revised form
21 January 2019
Accepted 26 March 2019
Available online 10 April 2019
Handling Editor: Nick M W Roberts

Keywords:
Palaeoenvironment
Carbonate chemostratigraphy
Shallow-water carbonates
Diagenesis
Kimmeridgian

ABSTRACT

Shallow-platform settings with marked differences in paleoplatform bottom physiography influence the degree of connection with oceanic waters and overall circulation patterns, even when sharing the same palaeoclimatic conditions. Two Kimmeridgian shallow-marine settings have been explored to test the sensitivity and reliability of carbonate chemostratigraphy to detect such differences. An integrated overview of the obtained elemental trends depicted four major facies, shared along specific stratigraphic intervals of both depositional records. Diagenesis obliterated original geochemical signals only throughout the siliciclastics-rich interval, corresponding to the most landward setting. For the remaining facies, elemental features could be attributed to the differential action of forcing mechanisms operating along the south-Iberian paleomargin during Kimmeridgian times. The highest degree of continental influence can be recognized by a strong relationship between Fe and Mn for the most proximal setting, which fades out along the mixed carbonate-fine siliciclastic rhythmic deposition in more open settings. A characteristic geochemical signature of progressively more positive $\delta^{13}C$ values and significantly higher Sr content is identified for the interval dominated by biogenic sponge buildups. Such a local response is related to local forcing by upwelling in the surroundings of a coral fringe. The geochemical signature of a hydrothermal origin can be clearly differentiated from the influence of mere terrigenous pulses. Accordingly, the decoupling of Fe and Mn along marginal settings is the clue to detecting major events of palaeogeographic restructuring. Observed temporal variations in Mg content along both studied sections are attributed to tectonic activity influencing nearshore/coastal water masses. By integrating chemostratigraphic information and complementary evidence, the palaeoenvironmental mechanisms promoting differentiated sedimentary records along ancient subtropical, shallow, coastal settings can be disentangled.

1. Introduction

Sea-water properties and related palaeoenvironmental dynamics are key features for characterizing ancient neritic, shallow marine water-masses. Chemostratigraphy is a fast-growing and promising tool for approaching palaeoenvironmental conditions along shallow settings (Parente et al., 2007; Sessa et al., 2012; Coimbra et al., 2016, 2017; Godet et al., 2016; Andrieu et al., 2017; Huck et al., 2017). This approach must be made thorough lithofacies and eco- and biochronostratigraphic analyses in order to bypass the intrinsic complexity of chemostratigraphic signals of carbonates in these settings.

The presented research approaches the potential of carbonate chemostratigraphy to disentangle the complex palaeoenvironmental evolution recorded along two shallow-water sedimentary sections encompassing Kimmeridgian times (ca. 157.3 ± 1 Ma to 152.1 ± 0.9 Ma ago; Cohen et al., 2013 updated; Ogg et al., 2016). Globally, this period is characterized by long-term rising sea-levels (Haq et al., 1987; Hardenbol et al., 1998) and wide carbonate/carbonate-siliciclastic shelves in Europe. A warm-

* Corresponding author. Dpto. Geociências, Universidade de Aveiro, Campus de Santiago, 3810-193 Aveiro, Portugal.
E-mail address: rcoimbra@ua.pt (R. Coimbra).
Peer-review under responsibility of China University of Geosciences (Beijing).

https://doi.org/10.1016/j.gsf.2019.03.006

temperate zone extended to 60° N–S latitude (Sellwood and Valdes, 2006), with inter-tropical to warm-temperate zones showing mean values of marine water temperature ranging from 12 °C to 25 °C, as derived from O-isotope values from fossil skeletals (bioclasts) and bulk micrite (Price and Sellwood, 1994; Caracuel et al., 1997; Lécuyer et al., 2003; Wierzbowski, 2004; Coimbra et al., 2009, 2014; Coimbra and Olóriz, 2012a,b; Colombié et al., 2014). However, despite this clear global picture, coeval shallow-platform areas fail to provide straightforward or equally informative records. This is because they are often afflicted by a combination of factors including, but not limited to: multiple sedimentary sources; the potential superimposition of global and regional climatic signals; the incompleteness of the sedimentary record, often more prone to diagenetic imprint; and a high sensitivity to local conditions. In such a context, understanding how the geochemical record of carbonates responds to these intrinsic complexities is key to providing a more comprehensive overview of carbonate platform differentiation in time and space.

Two study areas were chosen in order to compare neritic, shallow marine water-masses and palaeoenvironmental conditions during Early Kimmeridgian times in two relatively distant segments of the south-Iberian paleomargin. These comprise the Rocha Poço section in the eastern Algarve Sub-basin, nearby the eastern extreme of the Hispanic Corridor; and the Puerto Lorente section eastwards in the central Prebetic (Figs. 1 and 2). These selected sections show different tectonic contexts and lithofacies in the Lower to earliest Late Kimmeridgian (Platynota through lowermost Acanthicum zones in ammonite biochronostratigraphy, 156 Ma to 154.3 Ma; Ogg et al., 2016) and can serve to highlight the occurrence of a wide array of palaeoenvironmental conditions in epicontinental, shallow marine seas. A shared regressive trend from the Early–Late Kimmeridgian to late Jurassic–earliest Cretaceous times evidences a tectonic counteracting of long-term eustasy in epicontinental areas of the south-Iberian paleomargin (Marques et al., 1991). The aim is to make apparent how geochemical differences, allied with palaeoecological, sedimentological and stratigraphical interpretations, provide key information to depict differences in platform configuration, circulation patterns, seawater properties and other potential driving mechanisms responsible for differential palaeoenvironmental evolution in subtropical, shallow, coastal settings.

2. Studied sections, geological setting and palaeoenvironmental context

The two epicontinental sections chosen rely on a tight biochronostratigraphic control and present optimal outcrop conditions (Figs. 1 and 2). The Rocha Poço section—representative of epicontinental deposits along the SW Iberian palaeomargin, located in the eastern Algarve Sub-basin in southern Portugal (Fig. 2A,B)—is structured by N–S strike-slip faults and E–W extensional faults and flexures, showing irregular bottoms related to salt tectonics (Mannupella et al., 1988). Eco-sedimentary conditions in this sub-basin differed from those in the western Algarve Sub-basin, representing a persistent, shallow carbonate shelf-system throughout the Jurassic, with an assumed linkage to southern equivalents identified offshore in boreholes and connected to open-marine Tethyan epioceanic waters to the southeast (Marques and Olóriz, 1989a) (Fig. 1A,B).

Changing facies and stratigraphic discontinuities are common in Oxfordian and Lower Kimmeridgian deposits in the eastern Algarve Sub-basin (Marques and Olóriz, 1989b), indicating a mid-shelf palaeoenvironmental setting belonging to a neritic shelf-system characterized by common bioherms with sponges and/or corals (Marques, 1985; Ramalho, 1985; Rosendhal, 1985; Leinfelder, 1993). This evidences a local variability in nutrient levels over time, among other palaeoenvironmental forcing factors. Afterwards, marine inner-shelf conditions and homogenized sedimentation preceded a peak-regression during latest Jurassic–earliest Cretaceous times (Marques, 1985; Mannupella et al., 1988; Marques and Olóriz, 1989b).

The investigated Rocha Poço section shows two well-marked stratigraphic intervals (Figs. 2B1–B3 and 3A–D): 20 m of silty limestones and marls followed by 28 m of spongiolitic limestones and related facies (Peral and Cerro da Cabeça Formations) (Marques, 1985; Ramalho, 1988). At the lower part of the spongiolitic interval a third stratigraphic interval (20–28 m) can be highlighted on the basis of sponge-buildup development (Fig. 3B). Without latitudinal difference between the Algarve Basin and the central Prebetic Zone, local tectonics during the Early Kimmeridgian were very distinctive. This resulted in high bottom irregularities due to salt tectonics in the eastern Algarve Sub-basin and differential subsidence for mixed carbonate-siliciclastic rhythmites

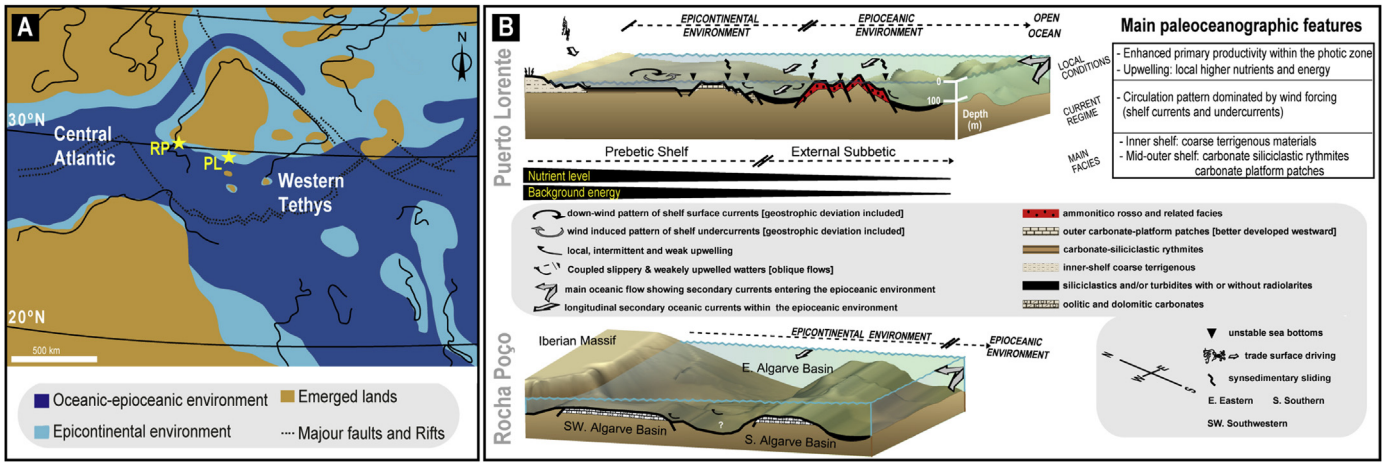

Figure 1. (A) Late Jurassic palaeogeography along western Tethys. Plate tectonics after Stampfli and Borel (2002) and depositional environments after Thierry et al. (2000a,b). (B) Simplified schematic representations of the southern Iberian palaeomargin showing assumed location of the studied sections at Puerto Lorente and Rocha Poço (adapted from Marques and Olóriz, 1989a and Coimbra et al., 2015). Evidenced palaeoenvironmental parameters during deposition are adapted from Olóriz (2000) and Coimbra et al. (2015).

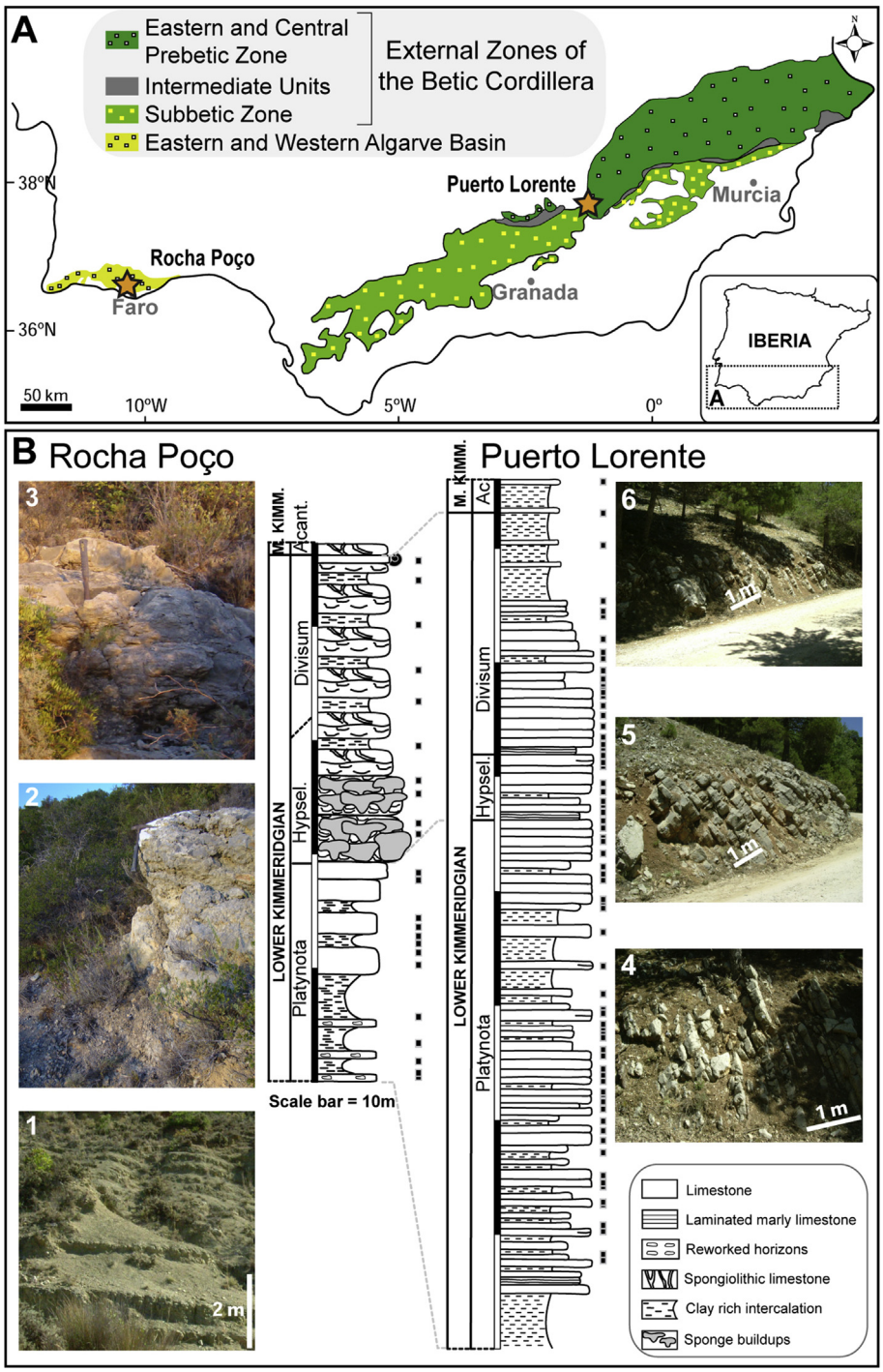

Figure 2. Selected epicontinental sections located in S Portugal and S Spain. (A) Regional distribution of geological units along the Betic Cordillera and the Algarve Basin, adapted from García-Hernández et al. (1980) and Marques et al. (1991), with geographic location of the studied sections Rocha Poço and Puerto Lorente (marked by stars). (B) Stratigraphic representation of facies variability and sample distribution along with representative field aspects: (1) siliciclastic interval at Rocha Poço; (2) sponge buildups at Rocha Poço; (3) spongiolithic limestone at Rocha Poço; (4–6) typical succession of limestone beds at Puerto Lorente section. Dashed lines indicate comparable time windows at the two sections (see text for further details). Note relevant lithostratigraphic differences within each section and also between sections.

in the Prebetic, where local Early Kimmeridgian synsedimentary sliding of Platynota Chron age deposits occurred in outer-shelf areas corresponding to the comparatively distal Internal Prebetic (Olóriz and Rodríguez-Tovar, 1998).

Kimmeridgan deposits in the Puerto Lorente section (Figs. 1 and 2) are typical for the Cazorla sector in the Prebetic Zone, and represent eco-sedimentary conditions of mid-shelf shallow-marine waters—External Prebetic—belonging to the epicontinental shelf-system of the Betic Cordillera (Fig. 1). The latter was a low-energy, eastward expanding and distally steepened ramp whose outer shelf corresponded to the Internal Prebetic (subdivision of the Prebetic Zone following Azéma et al., 1979 and García-Hernández et al., 1980). Shelf-break and steepened south to south-eastward slope separated epicontinental and epioceanic waters and eco-

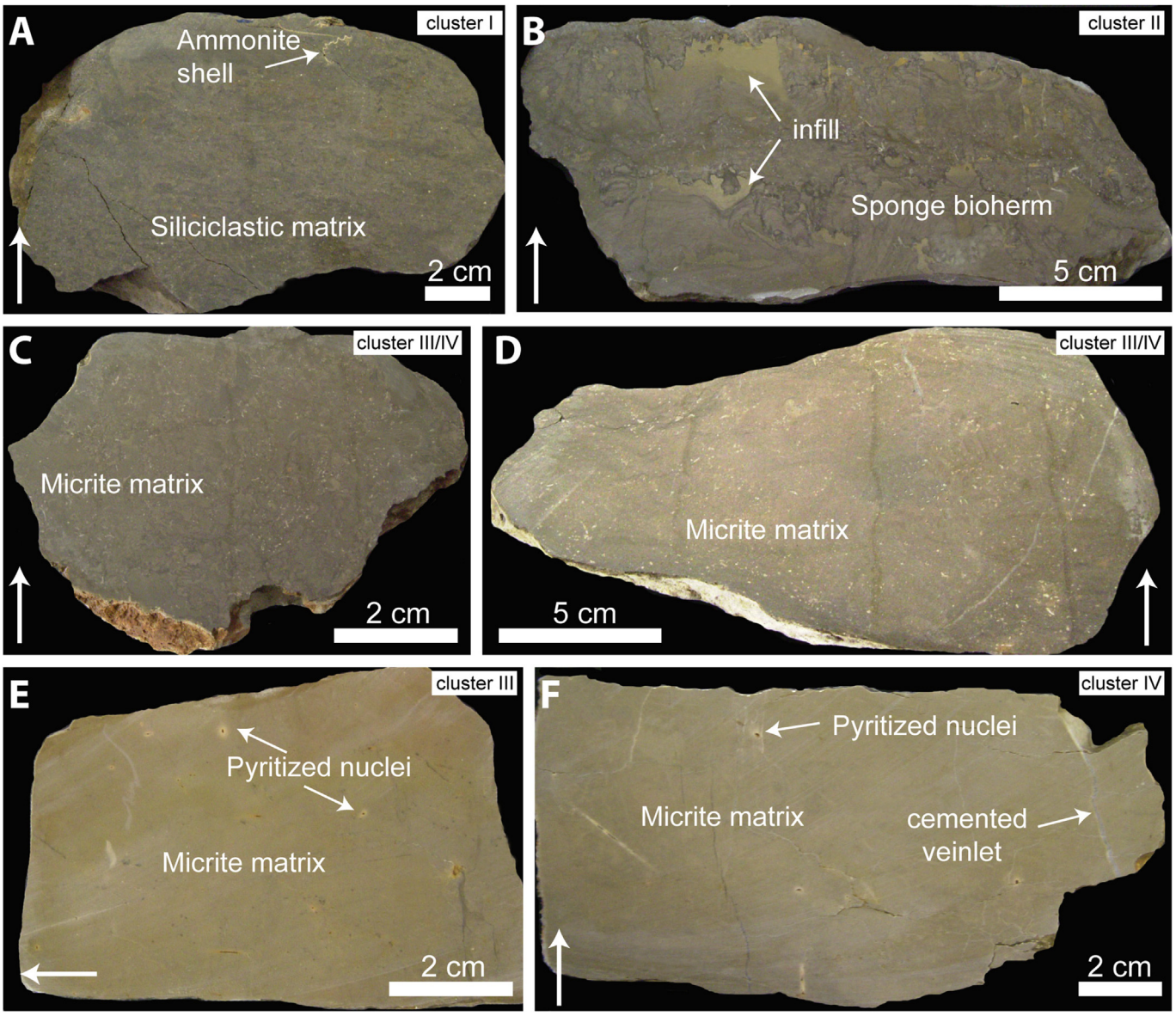

Figure 3. Representative features of polished slabs from both studied sections. (A) Siliciclastic samples from the Rocha Poço section. (B) Sample from the sponge-buildup interval at Rocha Poço. (C,D) Spongiolithic limestone samples from Rocha Poço section. (E,F) General aspect of limestone samples at the Puerto Lorente section, representative of the lower and upper portions of the section, respectively. Note the rather homogeneous aspect of the latter. Cluster numbers (I–IV) according to Fig. 5.

sedimentary domains, the latter being first represented by the adjacent, northernmost trough —the Intermediate Units— and then by the northern NE–SW swells-and-troughs complex belonging to the front of the allocthonous Subbetic Zone (Olóriz et al., 2002 for extended treatment). The Puerto Lorente section represents deposition on a comparatively raised bottom, resulting in condensed, hiatal deposition during Oxfordian and Earliest Kimmeridgian times (Bimmamatum pro parte and Planula chrones). Afterwards, an Early Kimmeridgian 3 m-thick siliciclastic intercalation—at the lowermost Platynota Zone—is significant since it is a typical outcrop feature (Fig. 2B) used as a regional reference level for correlation. It corresponds to the local record of a widely recorded tectonic pulse in the Iberian subplate—related to abrupt increases in the subsidence rate (Acosta, 1989)—also identified in northwest Africa and Submediterranean Europe (Marques et al., 1991; Leinfelder, 1993; Aurell et al., 2002; Colombié et al., 2014). Overlying it is a rather thick (over 100 m) homogeneous succession (Figs. 2B4–B6 and 3E, F) comprising a marly and silty limestone rhythmite (Lorente Fm.; Pendas, 1971). This succession was deposited under a warm climate with slight changes in the evaporation:precipitation ratio, as indicated by clay mineralogy studies (López-Galindo et al., 1994). Stratal-pattern analysis points to tectono-eustatic forcing at the bottom, with orbital forcing of mainly long- and short-term eccentricity and precession rather than obliquity cycles as a background control on sedimentation, especially in the middle part, and interacting with eustasy in the upper part (Olóriz et al., 1992; Olóriz and Rodríguez-Tovar, 1998). Mineralogical analysis revealed the influence of bottom topography on clay mineral distribution (López-Galindo et al., 1991).

Eco-sedimentary conditions of the substrate—mixed and transitional layers—in Puerto Lorente section indicate dominant dysaerobic, soft-to-firm water-sediment interphases, submitted to occasional erosion/omission favouring opportunistic colonization dominated by depositivorous/sedimentivorous organisms

(*Chondrites* makers; Olóriz and Rodríguez-Tovar, 1999). Unstable, relatively higher-energy seabeds were colonized by opportunistic suspension-feeders in scape galeries (large deep-tier *Diplocraterium* makers; Olóriz and Rodríguez-Tovar, 2000) with truncated tops related to erosion events. The scarcity of benthos was partially due to amensalism (Olóriz and Rodríguez-Tovar, 1999) as revealed by opportunistic, low-diversified ichnofossil suites dominated by the mining-like feeding of depositivorous/sedimentivorous, worm-like, endobenthic, probably chemosymbiotic but unconclusively identified organisms (*Chondrites* and *Planolites* makers such as nematodes, polychaetes or pogonophorans for the former, and polychaetes with diverse feeding behaviour for the latter). Scarce, large sized *Thalassinoides* were linked to oxygenation events (Olóriz and Rodríguez-Tovar, 1999). Notwithstanding, their deep reticulated branching without evidence of vertical tubes having associated sediment-mounds cannot be conclusively interpreted in terms of revealing erosion (Thalassinidean decapods build burrow openings with and without mounds, which help when interpreting trophic, ecological behaviours).

For the Rocha Poço and the Puerto Lorente sections, ecostratigraphic interpretations were approached based on fossil assemblages of macro-invertebrates with and without reference to sequence stratigraphy (Olóriz et al., 1988, 1991, 1993, 1994; Olóriz, 2000 and references therein). Based on the relative contents in benthic assemblages vs. ammonites, and the relative composition of the latter, faunal compositions and trends compatible with neritic, mid-shelf environments are revealed in both these sections. Irrespectively of sample size (50–1100 specimens) and local ecological-taphonomic effects, macroinvertebrate assemblages throughout the Lower Kimmeridgian are coherent with environmental conditions expected for decreasing (Platynota and Hypselocyclum biochronozones) and increasing ecospace (Divisum biochronozone) in correspondence to a regressive-transgressive cycle. Hence, major deviation in ammonite assemblages is seen in the upper Platynota Zone (comparatively unfavourable conditions at Rocha Poço); scarce ammonites (Puerto Lorente) and spongiolitic facies (Rocha Poço) are recorded in the Hypselocyclum Zone; and ecospace recovery for ammonites (Puerto Lorente) and spongiolitic facies punctuated by a short ammonite incursion (Rocha Poço) are typical records in the Divisum Zone.

The stratigraphic correlation between the Rocha Poço and Puerto Lorente sections derives from biochronostratigraphic control based on ammonite biostratigraphy (Marques, 1983; Marques and Olóriz, 1989a, 1992; Olóriz and Rodríguez-Tovar, 1993), here refined in order to provide a well constrained time-control (Fig. 2B). Accordingly, the ammonite records of *Sutneria platynota*, *Crussoliceras divisum*, *Orthaspidoceras uhlandi* and *Taramelliceras compsum*, and associated fauna, were used to support biochronostratigraphic correlations at the biozone-subbiozone levels.

3. Materials and methods

From a total of one hundred hand-samples, 86% correspond to carbonate-rich facies (>75 wt.% $CaCO_3$), including all the samples from the Puerto Lorente section and spongiolithic limestone samples from the Rocha Poço section (sampling resolution in Fig. 2). Conversely, lower carbonate contents were obtained for the siliciclastic interval recorded at the bottom of the Rocha Poço section (52–75 wt.% $CaCO_3$). This approach therefore covers the high lithological variability of the studied sections. Clay-rich intercalations were avoided due to limitations regarding microfacies analysis and the acquisition of the geochemical proxies here under scope (C- and O-isotopes and elemental data). Freshly cut surfaces were used for petrographic inspection and geochemical analysis. Thin sections were produced from each sampled horizon, and corresponding photomicrographs were used for microfacies characterization and to estimate the percentage of quartz grains throughout the siliciclastic interval identified at the bottom of the Rocha Poço section by means of pixel counting (see Coimbra and Olóriz (2012) for details on this method). Bulk rock powder samples of matrix micrite from carbonate-rich levels of both sections, spongiolithic limestones and silty matrix from some horizons of siliciclastic intercalations from the Rocha Poço section were hand-drilled using a 1 mm diamond drill tip. Care was taken to avoid atypical features such as fractures or stains.

Bulk micrite samples were analysed for their elemental content (Ca, Mg, Sr, Fe, Mn) and light stable isotope ($\delta^{13}C$ and $\delta^{18}O$) ratios at the Institute for Geology, Mineralogy and Geophysics (Ruhr University Bochum, Germany). Geochemical data from the Rocha Poço section, representing 24% of the total dataset, are taken from Coimbra et al. (2014, 2015, see for further details), here revisited under a completely new perspective. Carbon and oxygen isotopes were obtained for all the carbonate samples (including different facies) with a Thermo Fisher Scientific Gasbench II carbonate device connected to a Thermo Fisher Scientific Delta S Isotope Ratio Mass Spectrometer (following McCrea's (1950) method). Aliquots of the same samples measured for isotopic analysis were also investigated for their Ca, Mg, Sr, Fe, Mn and Ba elemental composition using inductively coupled plasma-atomic emission spectrometry (ICP-AES). Dissolution of 1.5 mg of the powdered sample in 1 mL of 3M HNO_3 (over 12 h) was followed by further dilution adding 2 mL of distilled water. After acid treatment, in some cases it was still possible to detect the presence of insoluble residue, corresponding to non-carbonate materials belonging to the detrital fraction as clay minerals and/or other Fe-bearing mineral phases (oxyhydroxides). This non-carbonate fraction is partially leached, but not completely dissolved during acid treatment of bulk micrite samples, which are the focus of the performed geochemical analysis. It was therefore necessary to filter the samples (Coimbra et al., 2015). Following this protocol, normalizing obtained elemental values (in ppm) by their calcium content ensures an adequate overview of the elemental dataset. Shared stratigraphic trend for both curves is therefore indicative of minimal leaching, evidencing the prevalence of carbonate-bound elements (Christ et al., 2012; Coimbra et al., 2015, 2017).

In order to combine the geochemical information retrieved from both sections, a hierarchical cluster analysis was performed for stable C- and O-isotope data and elemental concentrations. Cluster analysis algorithms made it possible to gather samples in groups (clusters) based on their degree of similarity. The resulting dendrogram representation was easier to interpret than the intricate variability of the raw dataset. For the specific case under focus, no impositions were made regarding the number of clusters obtained or truncation level. In this way, the obtained results are solely based on the level of entropy generated within each group, not influenced by user intuition or previous knowledge. The agglomeration was performed using the Ward method, with Euclidean distance. Since no difference was identified when standardized variables were tested against absolute values (in ppm), the latter were preferred.

The obtained geochemical information will be contrasted with previous knowledge, including palaeoecological, sedimentological and stratigraphical interpretations (brought forward in section 2). Integrating independent evidence provides support to geochemical interpretations, while demonstrating the potential enclosed in ancient shallow-water carbonate deposits.

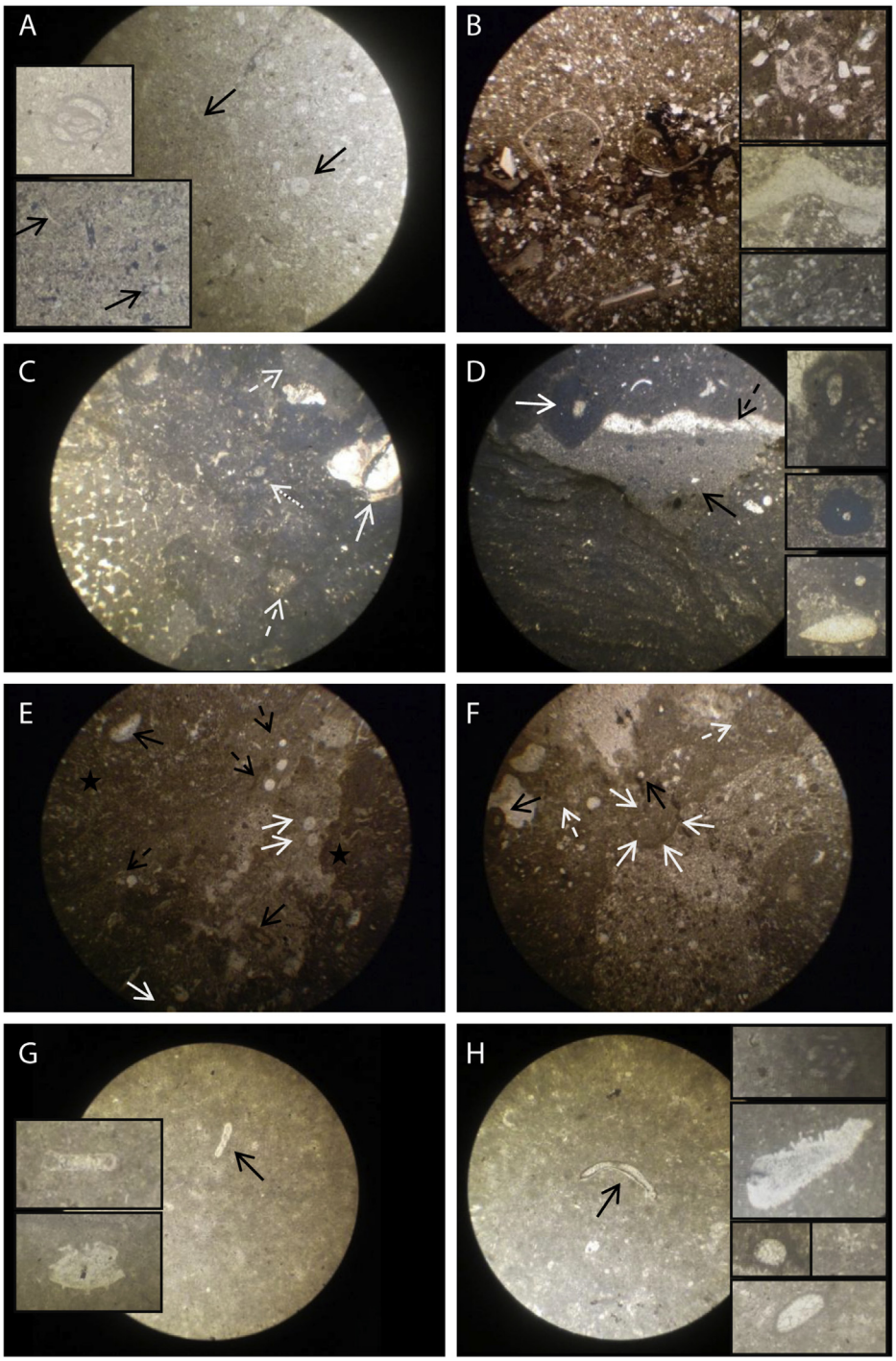

Figure 4. Microfacies details representative of both studied sections, Rocha Poço (RP) and Puerto Lorente (PL). (A) Dominant medium silt-to-fine sand size quartz, and less common fine sand deposit with comminuted skeletals. Wackestone poor in bioclasts of fine sand size, with scarce forams (*Lenticulina*?, miliolids –left upper close-up view) and rare zoospores of planktic algae (*Globochaetes*) and filaments (arrows and left lower close-up view) (RP-1x10). (B) Dominant medium silt-to-fine sand quartz and lithoclasts with common fine sand mud peloids and less common coated grains. Wackestone with rare subhorizontal concentration of skeletals (RP-13x3.5). Close-up views of undeterminable benthic foram (upper-right, RP-9x10), Microconchida attached to the inner surface of a bivalve fragment (center-right, RP-4x10) and miliolid foram (*Quinqueloculina*?, lower-right, RP-4x10). (C) Spongiolitic limestone showing hexactinellid sponge frame (left) and clotted microbial-algal fabric (right) with transverse sections of sponge spicules, coated benthic forams (dotted arrow), peloidal dense micritic aggregates, reworked aragonitic serpulid-like tubes (white arrow for geopetal orientation) and whitish interstitial (dissolution?) spaces (dashed white arrow) in-filled by allomicrite?, comminute particles, and peloids (RP16x3.5). (D) Dome-like agglutinated stromatolite showing irregular trapping of micropeloids (down-left); whitish interstitial space with geopetal filling of micropeloids and comminute particles (centre-up arrow); overlying open-space (coarse sparite, dashed arrow) fossilized by very fine dense microbialite matrix containing bivalve fragments, sponge spicules and coated comminute particles (RP-16x3.5). Close-up views of *Shamovella* (*Tubiphytes*) and medium sand size cryptic micrite BMC-micro oncoids (top-, center- and bottom-right) (RP-17x3.5 and RP-15Bx3.5), and coarse sand sized recrystallized bivalve (bottom-right) (RP-17x3.5). (E) Microbial (cryptalgal) fabrics with common thrombolitic structures (shaded white arrows in F); within microbialite clotted fabric (black stars) and inside inter-microbialite growth space (whitish), partially in-filled by fine siliciclastics and recrystallized carbonate showing peloidal micrite and small microbialite fragments; note zoospores of planktic algae (*Globochaetes*) showing axial cross between crossed nicols (white arrows); thinner cryptalgal growths around of wide ovoid-to-circular recrystallized nuclei (black arrows); transversal sections of uncoated sponge spicules (dashed black arrows). (F) Microbial (cryptalgal) fabrics with common thrombolitic structures (shaded white arrows), cryptic micrite BMC-microoncoids or lumps (white arrows), and thinner cryptalgal growths around of wide ovoid-to-circular recrystallized nuclei (sponge spicule the

4. Results

4.1. Petrographic analysis

In terms of microfacies features, the siliciclastic interval at Rocha Poço (Fig. 4A, B) revealed the presence of abundant angular quartz grains with an average abundance of 34% (established by pixel counting) and carbonaceous remains. Silty mudstone to wackestone matrices intercalate with more siliciclastic intervals, showing fossil remains of ammonites, bivalves and plants together with ostracods, and less common small benthic foraminifera (agglutinated and calcareous forms) and gastropods.

These features clearly contrast with those typically registered throughout the spongiolithic limestone interval of the Rocha Poço section (Fig. 4C–F), where microbial–cryptalgal–fabrics with abundant thrombolites dominate in spongiolithic horizons, together with micro-oncoids, thinner cryptalgal growths around wide ovoid-to-circular recrystalized nuclei and *Tubyphites*. Cryptalgal growths also coat around nuclei undifferentiated from the surrounding pale-grey matrix typical of interstitial spaces (potential inner cast of bivalves?, burrows?). Zoospores of planktic algae occur within the clotted fabric of microbialites as well as inside inter-microbialite growth space, which is partially in-filled by fine siliciclastics and recrystallized particles, peloidal micrite and small microbialite fragments. Sponge spicules and sponge frames are common. Geopetal in-filling can be identified through peloidal clots and small intraclasts embedded in irregular patches of microspar. Rare brachiopods and benthic agglutinate forams (single *Ammobaculites*-like lituolid) can be locally registered. Indeterminate bioclasts are very common.

At Puerto Lorente (Fig. 4G–H), the dominant texture consists of mudstone to wackestone with a rather low content in fossil remains, although some samples show an episodic increase in fossils (fossil-rich wackestone to packstone in condensed horizons). Silt-to-fine sand-size lithoclasts dominate, especially subrounded quartz, without distinction of sedimentary laminae and/or particular orientations of grains. The rather brownish matrix shows common mud peloids of medium silt size in mudstones (medium-to-coarse in wackestones) to very fine sand size, undetermined recrystallized particles of medium-to-coarse silt to very fine sand size, and comminuted skeletals of medium-to-coarse silt size. Carbonaceous particles occur. Fragmentation is high, and dissolution of skeletals and eroded particles is widespread. Examples of microboring and microbial-peloid coatings were identified. Macroscopic burrowing is concentrated in particular horizons. Common bioclasts range from medium silt (coarse silt in wackestone) to medium sand specimens and fragments, with rare very coarse sand-size fragments. They correspond to pelagic bivalves ("filaments"), echinoderm plates, bivalves, and ostracods, as well as benthic forams in-filled by matrix or recrystallized (e.g., epistominids, spirillinids, nodosariids), small calcispheres, zoospores of planktic algae, less common radiolaria, scarce brachiopods, echinoid spines, crinoid ossicles and arm plates, *Saccocoma* brachials, gastropods, corals, bryozoans, sponge spicules, belemnites and aptychi. Serpulids occur in stiffground horizons.

4.2. Statistic approaches to geochemical variables

Linear (Pearson) correlation among all tested geochemical variables obtained from carbonate-rich horizons was performed individually for each section (Table 1). The highest correlation coefficients ($R > 0.7$) were obtained exclusively when Fe and Mn concentrations are concerned (Table 1), and verified for both studied sections. At the Rocha Poço section, Fe and Mn also correlate very strongly with C-isotope values (Table 1).

The cluster analysis applied to all geochemical variables established a dendrogram with two main branches that generate four geochemical clusters (clusters I to IV, Fig. 5A and Table 2). The relative contribution of each variable accounting for the differences among clusters can be accessed along the profile plot of each cluster (Fig. 5B; centroid values in Table 2). Accordingly, $\delta^{13}C$ values and Fe concentration seem to have a greater influence in discriminating between clusters I and II, while Mg and $\delta^{18}O$ are visibly less relevant. Clear cases of these trends are also evidenced in Table 2, where for example the $\delta^{13}C$ centroid value is −2.2‰ for cluster I and 0.84‰ for cluster II, along with differences in Fe concentrations of ca. 6000 ppm vs. 3000 ppm (respectively, clusters I and II). In contrast, the geochemical differences accounting for the differentiation between clusters III and IV are much smoother (Fig. 5B and Table 2). While Mg and Sr abundance show rather similar values (Fig. 5B and Table 2), slight differences in Fe and Mn concentrations seem to best represent the contrast between these two clusters (Table 2).

The stratigraphic representation of the samples included in each cluster (Fig. 5C) shows that they are not randomly distributed. In fact, each cluster is well constrained across specific stratigraphic intervals (Fig. 5C). Interestingly, this differentiation follows only partially the most significant facies changes identified throughout both outcrops (Fig. 5C). Accordingly, cluster I corresponds to the lowermost interval at the Rocha Poço section (0–20 m; Platynota Zone), followed by cluster II (20 m to ca. 25 m; lowermost Hypselocyclum Zone). Both these clusters are exclusively represented along the Rocha Poço section, coinciding with the facies showing lower carbonate content (Fig. 5C). In contrast, facies with similar high carbonate content (Fig. 5C) are represented by two clusters (III and IV) at both sections. Cluster III dominates the first 40 m (throughout Platynota Zone) of the Puerto Lorente section, changing into cluster IV for the upper interval of this section (40–80 m; Hypselocyclum and Divisum biochronozones). Regarding the Rocha Poço section, clusters III and IV are interspersed in the uppermost 15 m of the section (mid-upper Hypselocyclum and Divisum biochronozones). For this reason, further considerations will use the combination of clusters III and IV for the Rocha Poço section.

smaller one?, black arrows); *Tubyphites* (not shown); cases of cryptalgal growths around nuclei undifferentiated from the surrounding pale-grey matrix typical of interstitial spaces; peloidal clots and small intraclasts in irregular patches of microspar that sometimes represent geopetal fillings. Not shown are rare brachiopods, scarce benthic agglutinate forams (single *Ammobaculites*-like lituolid), and indeterminate forms (E,F; RP-18x3.5). (G) Mudstone; medium silt-to-very fine sand size mud peloids; no lamination. From greater to smaller size, bioclasts are a single medium-sand size undetermined bioclast (left lower close-up view); rare medium to very fine sand-size pelagic bivalves ("filaments"); scarce fine sand-size benthic forams recrystallized (uncoiled nodosariid–arrow) or in-filled by matrix (rare spirillinids–left upper close-up view), and small recrystallized and disarticulated ostracods and/or bivalves?; very fine-sand to coarse-silt-size calcispheres; medium-to-coarse silt-size comminute skeletals and rare recrystallized particles (PL-35Ax10). (H) Wackestone; medium-coarse silt-to-very fine sand-size mud peloids with conminute recrystallized skeletals of medium-to-coarse silt-size and common recrystallized particles of coarse silt or very fine sand; no lamination. From greater to smaller size, bioclasts are rare very coarse sand-size eroded-bored echinoderm plate (right upper-center close-up view); medium sand-size benthic forams (scarce spirillinids and rare microbored disarticulated bivalves–arrow) and undetermined skeletals; rare fine-sand-size miliolids (*quinqueoculina* –right top close-up view), disarticulate valves of mall ostracods and/or bivalves?, and holothurian sclerites?; very fine to fine sand-size "filaments", rare small recrystallized stellate-pentagonal crinoid ossicles and "U"-arm microplates, common fragmented echinoderm plates, and relatively common microbial-peloid coating of recrystallized grains (voids?) (right lower-center, left close-up view) and isolate ostracod valves; and rare medium-coarse silt-to-very fine sand-size echinoid spines (right lower-center, right close-up view), fragments of gastropod?, and a single recrystallized zoospore of planktic algae (*Globochaetes*) (PL-75Cx10).

Table 1
Pearson correlation matrix for studied geochemical proxies. Bold lettering refers to statistically significant correlation coefficients (here >0.7).

		$\delta^{13}C$	$\delta^{18}O$	Mg/Ca	Sr/Ca	Fe/Ca	Mn/Ca
P. Lorente	$\delta^{13}C$	**1**					
	$\delta^{18}O$	0.27	**1**				
	Mg/Ca	−0.39	0.18	**1**			
	Sr/Ca	−0.28	−0.27	0.61	**1**		
	Fe/Ca	−0.50	−0.49	0.51	0.48	**1**	
	Mn/Ca	−0.49	−0.37	0.56	0.67	**0.82**	**1**
R. Poço	$\delta^{13}C$	**1**					
	$\delta^{18}O$	0.50	**1**				
	Mg/Ca	0.04	−0.10	**1**			
	Sr/Ca	−0.10	−0.34	0.37	**1**		
	Fe/Ca	**−0.78**	−0.45	0.46	0.34	**1**	
	Mn/Ca	**−0.73**	−0.25	0.16	0.47	**0.70**	**1**

In order to appraise the significance of the obtained geochemical clusters from horizons with variable carbonate content, the geochemical dataset was compared against well-known depositional and diagenetic trends (Fig. 6). The comparison between Fe and Mn concentrations at both sections provided a very high correlation coefficient ($R = 0.9$; Fig. 6A). Only two samples depart from this trend, corresponding to sharp Mn increments up to 600–800 ppm (Fig. 6A). When comparing O-isotope values with Mn concentrations for both sections, no significant correlation was obtained between these variables (Fig. 6B). However, two trends became apparent along this plot: a progressive O-isotope decrease from −2.5‰ to −5‰ from clusters IV to III; and decreasing Mn concentration from clusters I and II towards III and IV, without major changes in O-isotope values (Fig. 6B).

4.3. The geochemical dataset

The centroid values of geochemical clusters I to IV were compared to the distribution of the untreated dataset, i.e., across the C- and O-isotope crossplot (Fig. 7) and along stratigraphic elemental abundance (Fig. 8) to support further discussion.

4.3.1. C and O-isotope values

Distinct lithofacies in the two epicontinental sections (Figs. 2–4) show clear differences in carbon and oxygen isotope values (Fig. 7A). Regarding $\delta^{13}C$, samples from the siliciclastic interval at the Rocha Poço section show the lowermost values, ranging from −5.6‰ to 1.0‰. Samples belonging to this interval show an average 34% of quartz grains (example in Fig. 7B). The spongiolithic limestone $\delta^{13}C$ values at Rocha Poço provided values from 1.4‰ to 2.1‰, partially overlapping the very narrow range of values presented by samples from the Puerto Lorente section. The latter show very persistent values, ranging from 1.7‰ to 2.7‰ (Fig. 7A).

The siliciclastic interval at Rocha Poço shows the lowermost, narrowest range of $\delta^{18}O$ values, from −4.8‰ to −3.9‰. The remaining lithofacies show a wider range of variation in $\delta^{18}O$ values, both from ca. 4.8‰ to −2.4‰. Another evident feature is that the spongiolithic limestone facies show a stratigraphic increase in O-isotope values.

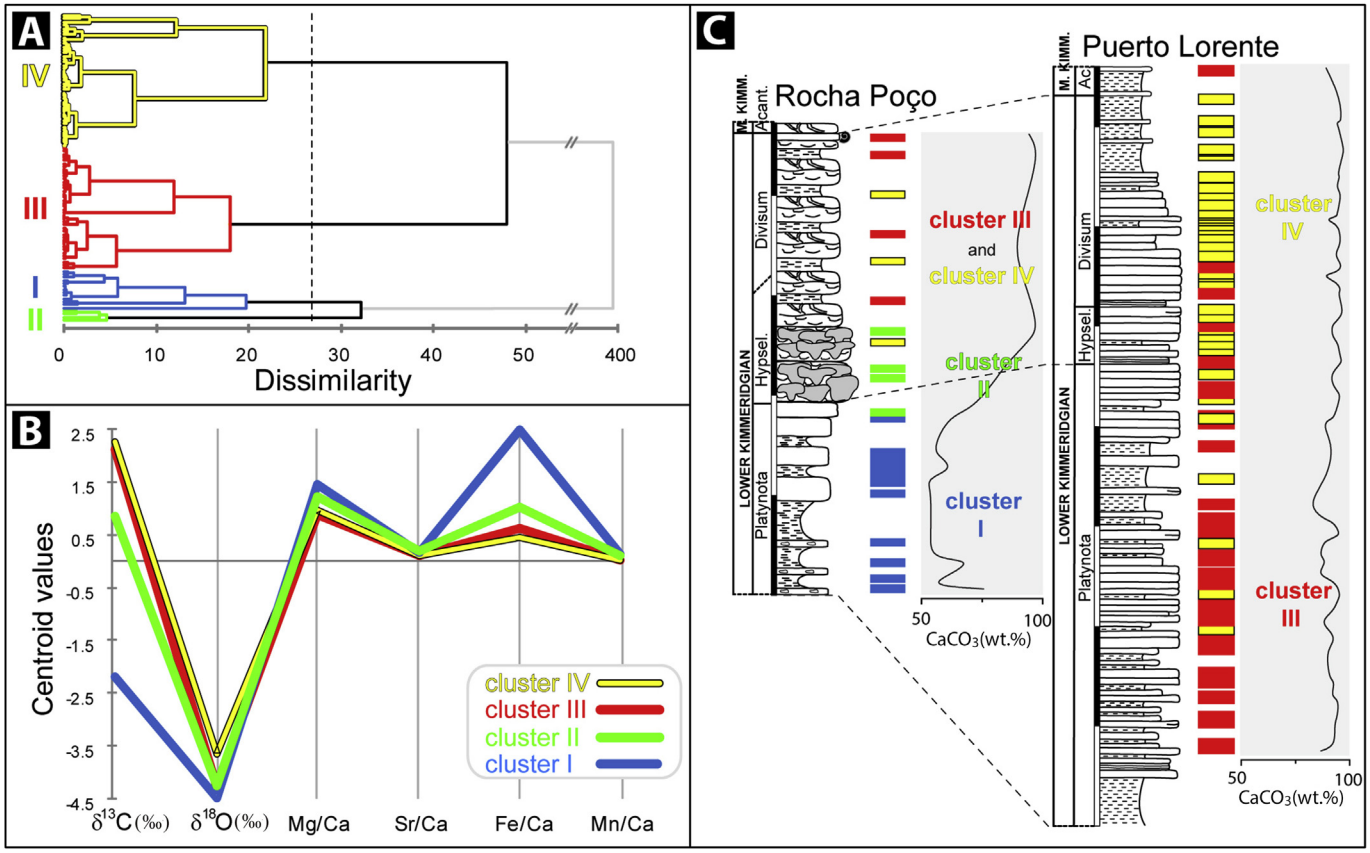

Figure 5. Agglomerative hierarchical clustering performed on the set of geochemical variables obtained for both sections. Vertical line marks the truncation level. (A) Dendrogram according to dissimilarity between samples, showing the establishment of two main branches and four clusters (clusters I to IV). (B) Profile plot for each geochemical variable representing normalized centroid value for each computed cluster (see also Table 2). (C) Stratigraphic distribution of samples assigned to each cluster and respective carbonate content ($CaCO_3$ in wt.%). Note the dominance of each cluster along specific stratigraphic intervals, despite gradational transition and/or episodic recurrences. The relation between each cluster and the carbonate content of the sampled horizons and lithofacies is only partial.

Table 2
Centroid values for each cluster, absolute values (in ppm) and normalized by calcium content (see also Fig. 5).

Cluster	$\delta^{13}C$ (‰)	$\delta^{18}O$ (‰)	Mg/Ca	Sr/Ca	Fe/Ca	Mn/Ca
I	–2.20	–4.48	1.4483	0.1541	2.4804	0.1397
II	0.84	–4.25	1.2361	0.1811	1.0182	0.0984
III	2.12	–4.29	0.8921	0.1001	0.6321	0.0298
IV	2.27	–3.65	0.9816	0.0978	0.4623	0.0261

Cluster	--	--	Mg (ppm) *	Sr (ppm) *	Fe (ppm) *	Mn (ppm) *	Ca (ppm)*
I	--	--	3361	362	5732	330	232,700
II	--	--	3916	574	3135	321	316,938
III	--	--	3215	361	2255	107	362,007
IV	--	--	3622	362	1690	96	370,261

*values used in Fig. 6

The centroid cluster values of C- and O-isotopes (Table 2) were used for positioning the obtained geochemical clusters along the obtained C- and O-isotope dataset (Fig. 6). Accordingly, cluster I falls along the siliciclastic interval of the Rocha Poço section, and cluster II records a transition between these facies and the uppermost spongiolithic limestone (Figs. 5C and 7A). In turn, clusters III and IV partially overlap the range of C- and O-isotope values presented by the spongiolithic limestones of Rocha Poço and all the Puerto Lorente samples (Fig. 7A). Along this trend, cluster IV shows a less negative centroid $\delta^{18}O$ value of −3.6‰ (Fig. 7A and Table 2).

4.3.2. Stratigraphic elemental composition

The elemental abundance along each section is presented in both absolute and corrected values (ppm and calcium normalization; Fig. 8). They largely overlap, confirming that all elements under scope were carbonate bound, discarding significant leaching of non-carbonate phases. This similarity justifies the use of ppm values, which is highly convenient for further discussion. The only exceptions are the cases of Mg and Sr across the siliciclastic interval at Rocha Poço (cluster I, Fig. 8B). Such a difference is probably due to the very low calcium content of this siliciclastic facies, 200–300 ppm (Coimbra et al., 2015; Fig. 5C), which induces considerable bias in the correction procedure (see section 3). Since values in ppm are preferable, this effect is held to be irrelevant.

The description of the stratigraphic elemental fluctuations (Fig. 8) will be based on the major elemental differences of each cluster (Table 2). Cluster I shows the highest Fe concentration (ca. 6000 ppm; Table 2 and Fig. 8B), along with high Mn values (ca. 300 ppm). Mg and Sr values are within the range of other established clusters (3215 ppm and 361 ppm, respectively), hence they are not considered a characteristic feature for this cluster. Cluster II is mainly characterized by a significant increase in Sr and Mg contents, reaching ca. 600 ppm and 4000 ppm, respectively (Fig. 8B and Table 2). This change is accompanied by a rather high Mn content (321 ppm), but lower Fe values (ca. 3000 ppm). When compared to clusters I and II, clusters III and IV show overall depletion in all measured elements (Fig. 8A,B; Table 2), more significant in the case of Mn and Fe concentrations. But when comparing clusters III and IV to each other, different trends arise (Fig. 8). Namely, Fe and Mn differences are not very noticeable, but still show a slight decrease from cluster III to IV; Sr content remains

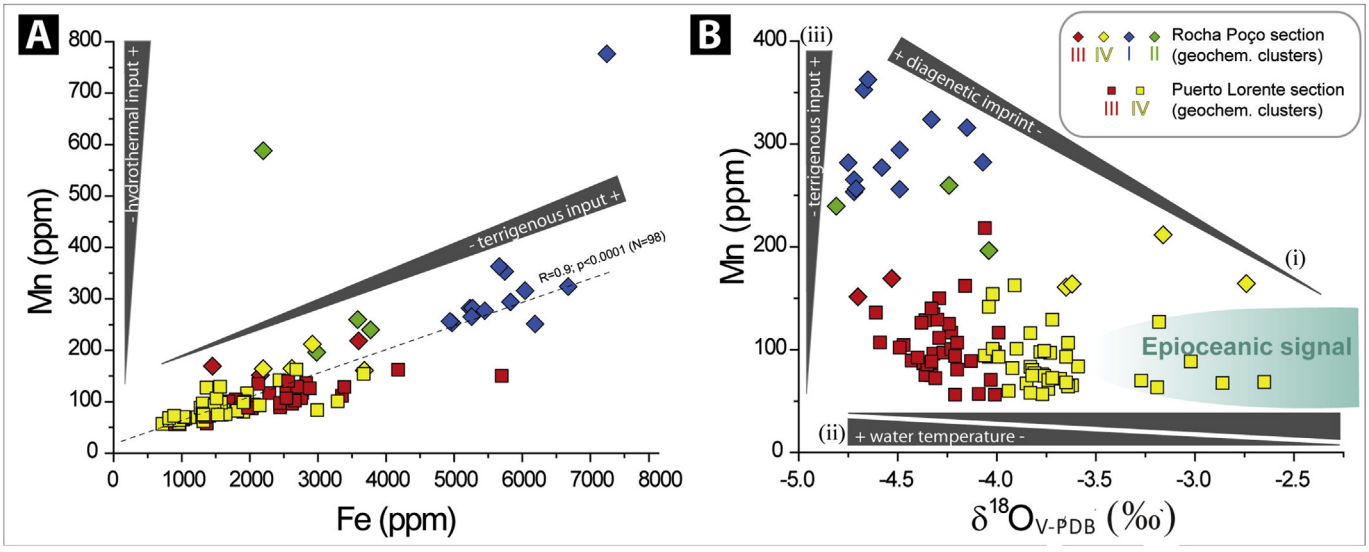

Figure 6. Geochemical biplots combining selected variables for both sections. (A) Iron versus Mn concentration, along with expected trends proposed for hydrothermal (Corbin et al., 2000) and terrigenous input (e.g., Vincent et al., 2006). (B) Obtained oxygen-isotope values versus Mn concentration, with indication of expected trends due to (i) variable degree of diagenetic influence (e.g., Veizer, 1983); (ii) salinity and water temperature changes (Marshall, 1992), as well as (iii) terrigenous input; epioceanic $\delta^{18}O$ range of values after Coimbra et al. (2015). See text for details on trends (i–iii).

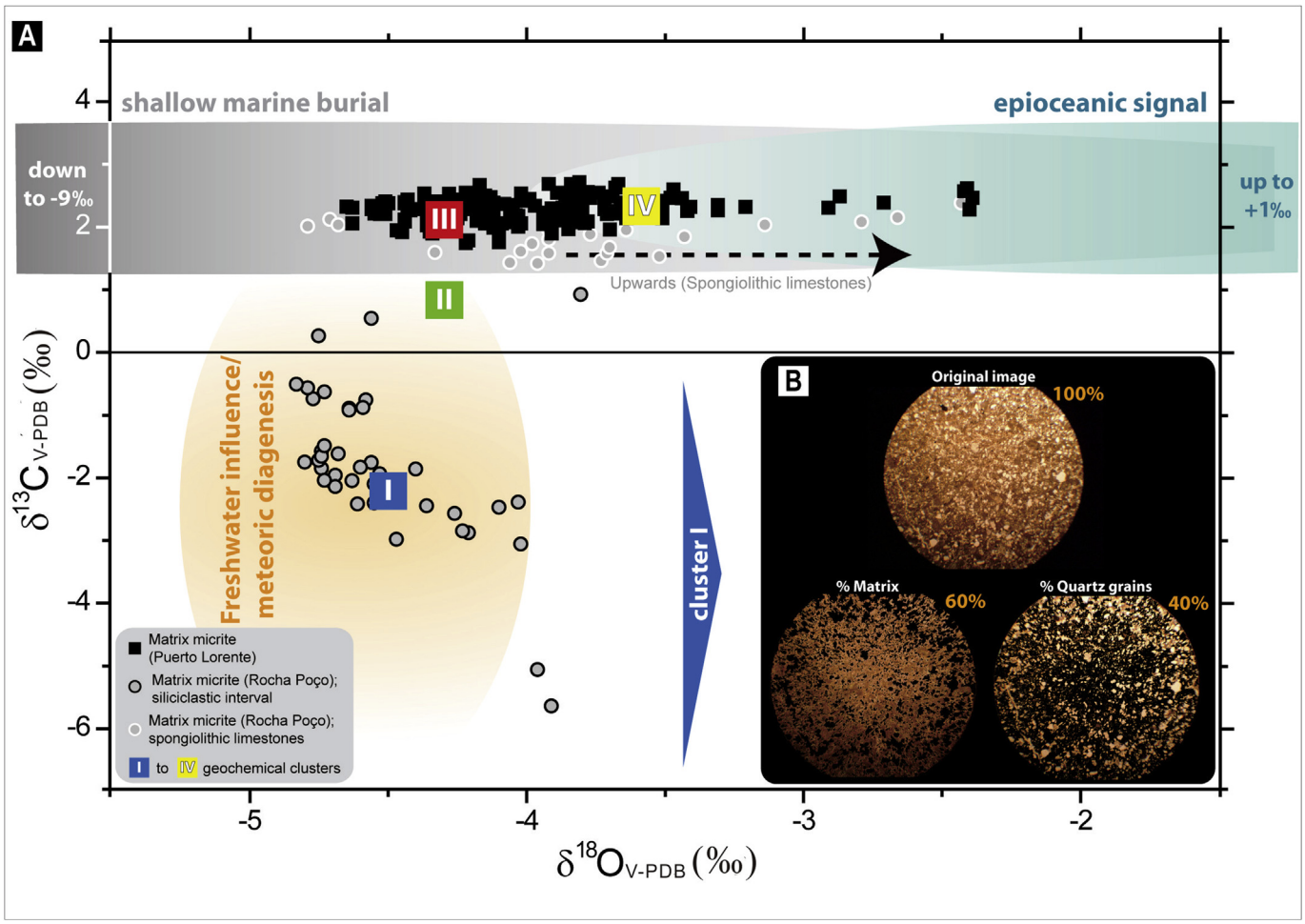

Figure 7. (A) Crossplot representation of carbon and oxygen isotopes obtained for the studied sections at Rocha Poço and Puerto Lorente. Note clear variations depending on lithology. Epioceanic signal and diagenetic (burial and meteoric) envelopes after Coimbra et al. (2014). (B) Example of quartz content estimation by pixel counting for samples belonging to the siliciclastic interval of the Rocha Poço section.

quite constant and Mg concentration is relatively higher in cluster IV (Fig. 8A,B).

Apart from the major stratigraphic elemental trends, particular peaks shown by certain variables are noteworthy (Fig. 8). These include Fe concentration-peaks reaching 6000 ppm, accompanied by coeval Mn increments (up to 160 ppm) along the Puerto Lorente section (at the bottom and ca. 30 m above; Fig. 8A). Also noteworthy are the sharp Mn concentration peaks (up to 800 ppm) that occur without major changes in Fe concentration at the base and mid-portion of the Rocha Poço section (Fig. 8B).

5. Discussion

Both studied sections represent neritic, mid-shelf environments, submitted to a regressive-transgressive cycle. But major differences can be highlighted (see section 2) and evidence from previous studies can be articulated with new geochemical data, and discussed in light of the obtained geochemical differentiation. Namely, the Rocha Poço section represents irregular bottom physiography along a persistent, shallow carbonate shelf-system throughout the Jurassic in SW Iberia (see section 2). This neritic mid-shelf setting received variable nutrient input, as clearly evidenced by a separation in the spatial distribution of coral and sponge dominate communities. Later, marine inner-shelf conditions and homogenized sedimentation preceded a peak-regression during latest Jurassic-earliest Cretaceous times. In contrast, the Puerto Lorente section represents low-energy, mid-shelf shallow-marine conditions to the southeast at the epicontinental shelf-system of the Betic Cordillera, dominated by dysaerobic, soft-to-firm water-sediment interphases, only occasionally submitted to erosion/omission. As a raised bottom, it received condensed, hiatal deposition during Oxfordian and oldest Kimmeridgian times. This was interrupted by a rather thin carpet of siliciclastics that resulted in a relative levelling of the seabed, corresponding to the local record of a widely recorded tectonic pulse in the Iberian subplate. It was immediately followed by the deposition of a thick, marly and silty limestone rhythmite under warm climate. Orbital forcing was the main control dictating the stratal pattern on this ramp, interacting with eustasy in the upper part of the record (see section 2).

When comparing the two studied sections, major paleoenvironmental differences at the Rocha Poço sector relate to more irregular bottoms and their influence on shallow marine currents. The common framework entails a relative disconnection from oceanic circulation, stronger continental influence, and higher biogenic activity on raised bottoms, either under oligotrophic conditions (coral fringe reefs) or locally submitted to fertilization by upwellings (sponge buildups and related facies). In such a context,

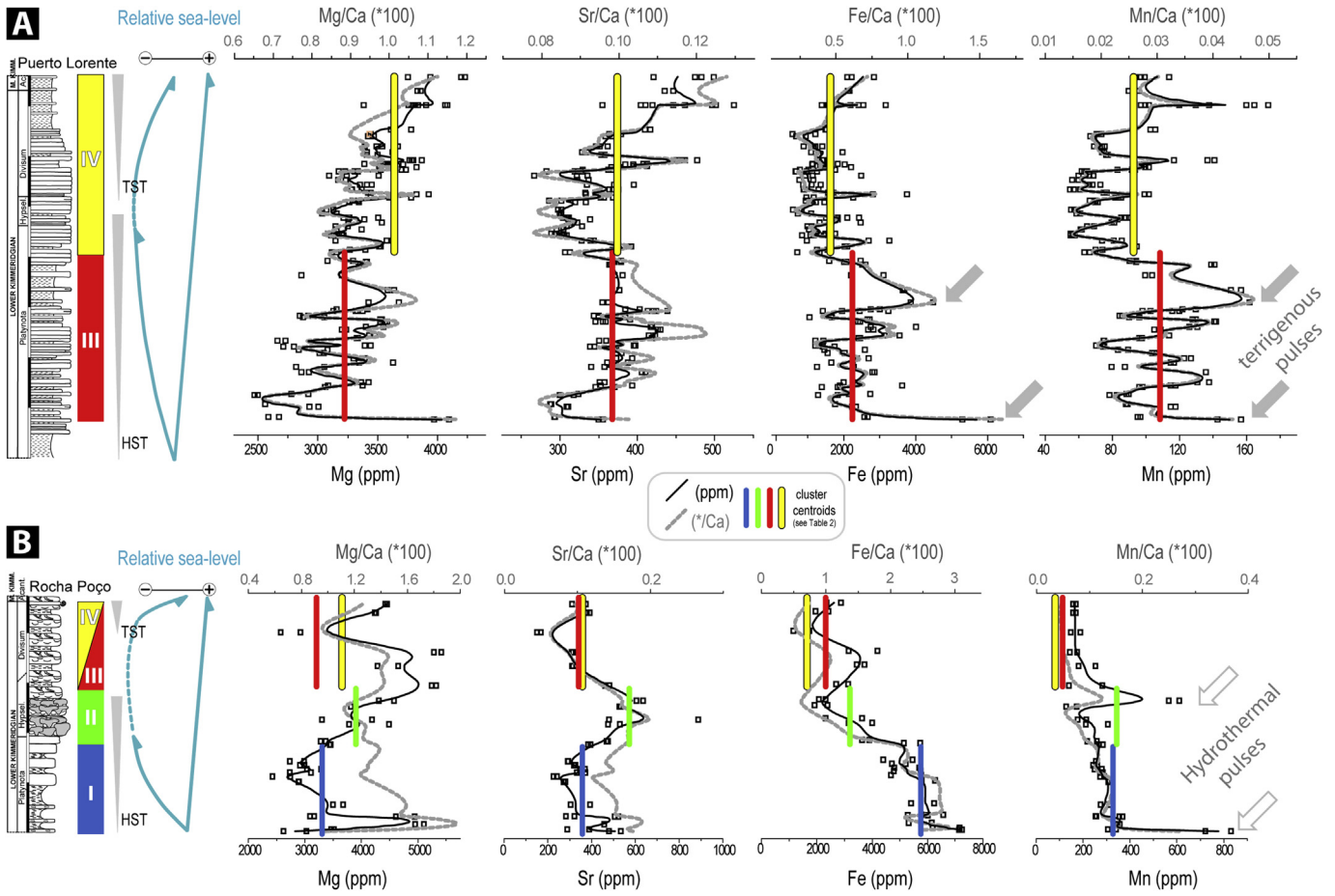

Figure 8. Stratigraphic trends of elemental variations of Mg, Sr, Fe and Mn throughout both studied sections along with indication of the geochemical clusters I to IV. (A) Puerto Lorente section, showing only slight differences between clusters III and IV. (B) Rocha Poço elemental record. Note relative differences in elemental concentration among the four obtained geochemical clusters. Absolute values (in ppm) are plotted along with corrected (calcium normalized) values for comparison, with overall agreement between both curves (b-spline curves are used to connect datapoints). Grey arrows along Fe and Mn curves indicate sharp increase in elemental concentration (see text for discussion).

biogenic activity was also higher at the seabed level, forcing a higher incidence of biogenic automicrite. Skeletal breakdown and drainage from the coral-fringe reef and the spongiolithic buildups resulted in a common skeletal-rich deposition (Fig. 3).

In contrast, the "homogeneous" rhythmic carbonate-fine-siliciclastic deposition at the Puerto Lorente sector is interpreted as resulting from a position comparatively seawards and distal from the potential carbonate factory, in a low-energy, ramp-like, non-rimmed shelf. Higher accumulation rates, as inferred from stratigraphic thickness, distinctive surfaces and lithofacies, show Puerto Lorente to be a comparatively persistent, lower-energy depocenter receiving finer continental detritus and offbank exportation of carbonate muds and siliciclastics, with a higher incidence of allomicrites. The established paleoenvironmental conditions will be discussed in terms of the geochemical information obtained.

The most significant correlations between geochemical variables for each section all included Fe and Mn (Table 1). When both sections are considered (Fig. 6A) the Fe vs. Mn correlation is very evident, fitting perfectly with independent evidence provided by the lithofacies differentiation resulting from field observations and the carbonate content of the materials under scope (Figs. 5C and 6A). Additionally, particular cases of deviation from the major Fe and Mn correlation are strongly evidenced (Fig. 6A). The coupling of these variables informs on the overall terrigenous input along both epicontinental areas (Elrod et al., 2004; Vincent et al., 2006; Zhao and Zheng, 2014; Costa et al., 2016; Coimbra et al., 2017). Such elemental supply is therefore more significant for the Rocha Poço section, especially for cluster I, representing the siliciclastic interval at the bottom of this section. The two samples departing from the major trend (bottom and 30 m above, Rocha Poço section; Fig. 6A) coincide with the bottom' of the siliciclastic interval and topmost horizon of the spongiolithic bioconstructions (Fig. 8B). These peaks in siliciclastic input clearly mark a sharp transition which can be attributed to local tectonic noise, agreeing thus with major geochemical forcing due to hydrothermal contribution, i.e., syn-depositional submarine volcanic activity. This activity is typically characterized by sharp Mn input without major Fe changes, among others (Lupton and Craig, 1981; Kickmaier and Peters, 1990; Rubin, 1997; Corbin et al., 2000; Aquilina et al., 2014; Coimbra et al., 2015). Such a difference is attributed to dispersal mechanisms of hydrothermal plumes, accounting for seawater Mn contamination up to great distances from seepage (Klinkhammer and Hudson, 1986; Feely et al., 1992; Middag et al., 2011; Coimbra et al., 2015). In contrast, Fe showing lower solubility in seawater tends to be removed from the hydrothermal plumes earlier, i.e., closer to the source (e.g., Bennett et al., 2008). Alternative proxies for such hydrothermal activity are not used due to the wide application of Mn to depict hydrothermal influence in ancient deposits and even detect plume progression in modern settings (Lupton and Craig, 1981; Kickmaier and Peters, 1990; Rubin, 1997; Corbin et al., 2000; Middag et al., 2011; Aquilina et al., 2014; Coimbra et al., 2015).

The variation of Mn concentration (excluding hydrothermal contribution) was used along with O-isotope values (Fig. 6B) to test for the influence of diagenetic processes on the geochemical dataset recorded at the investigated epicontinental sections. Although Mn/Sr is a commonly used ratio due to opposing partition coefficients (Brand and Veizer, 1980; Veizer, 1983), it was here avoided due to a potential bias induced by particular palaeoenvironmental behaviour of Sr (further discussed). Absolute manganese abundance was therefore preferred (Fig. 6B).

Such comparison led to a clear separation between: (i) diagenetic influence (Veizer, 1983; van der Kooij et al., 2009); (ii) changes in water-mass density related to salinity and temperature (e.g., Marshall, 1992); and (iii) variable terrigenous input (also depicted in Fig. 6A). In Fig. 6B, the diagenetic trend (i) is determined exclusively by samples from the Rocha Poço section, marked by progressive depletion in O-isotope values along with Mn increase towards the siliciclastic interval (cluster I; Fig. 6B). The O-isotope diagenetic pattern along siliciclastic facies was previously dealt with in Coimbra et al. (2014). Apart from the original volume of freshwater entering the proximal fringe (inner and middle shelf), the silty-to-fine sandy character of this more siliciclastic facies allows to assume higher porosity and permeability due to its comparatively low but variable carbonate content, thus promoting a higher water/rock ratio accounting for the diagenetic influence of phreatic (fresh/brackish) waters (Coimbra et al., 2014 for full details). This diagenetic pattern serves to demonstrate that, the depicted geochemical trends are in fact a combined effect of particular palaeoenvironmental differences, related to changes in water-mass density and terrigenous input (ii and iii in Fig. 6B), which later promotes differential, more pervasive diagenetic pathways.

Based on the above, samples belonging to clusters III and IV from both sections record a clear trend of increasingly negative $\delta^{18}O$ values (−2.5‰ to −4.5%; Fig. 6B) when compared to the coeval epioceanic signal (Fig. 7; epioceanic signal and burial/meteoric diagenetic envelopes after Coimbra et al., 2014). This relative depletion fits a scenario of increase in water temperature landward, towards epicontinental, more nearshore settings throughout Early Kimmeridgian times. The alternative of increased burial temperature is here discarded based on the integration of isotope and elemental data (Fig. 6B) and the lack of very negative burial realm oxygen-isotope values (down to −9‰) when compared to late cements belonging to coeval nearby settings (Fig. 7A). The potential record of this trend along other clusters may have been compromised by the previously mentioned diagenetic influence. In comparison, the obtained absolute $\delta^{18}O$ values for clusters III and IV demand an exaggerated difference in seawater temperature of ca. 8 °C (Marshall, 1992) between epioceanic and epicontinental water masses. Such an effect must therefore act in combination with decreasing salinity due to freshwater input landwards on the corresponding epicontinental areas. This interpretation reinforces previous evidence of freshwater/brackish influence on the geochemical record throughout the epicontinental realm (Coimbra et al., 2014), precisely due to a high original porosity (Fig. 7A). The latter is supported by the strong influence of terrigenous input (Fig. 6A,B and Table 1). However, it is important to note that the obtained geochemical data do not reflect original lithological differences or differential diagenetic processes affecting the mixed carbonate-siliciclastic rhythmite at Puerto Lorente (Fig. 2B), where siliciclastics are finer and restricted to a thiner stratigraphic interval of the same age. This is especially evident along the O-isotope record, showing a very persistent record across subtle lithological changes throughout time (Figs. 6B and 7). The temperature and salinity changes previously discussed are perhaps more significant, and hence superimpose other background influences. Since this study focuses mainly on carbonate horizons (Figs. 2 and 5), such fine-scale trends factors may be hard to detect.

The described trends will be taken into account together with the information obtained from geochemical clusters in terms of the palaeogeographic and palaeoecological contexts of the studied areas at Puerto Lorente and Rocha Poço. Cluster analysis resulted in a highest order major branching (dissimilarity) that differentiates clusters I and II from clusters III and IV (Fig. 5A). In addition, further differences between clusters I and II were detected along the profile plot of each cluster (Fig. 5B). For these reasons, the more differentiated clusters I and II will be discussed separately, while the more similar clusters III and IV will be addressed jointly.

5.1. Cluster I: the siliciclastic end-member

Cluster I, covering the siliciclastic interval along the Rocha Poço section, is the most differentiated one (Figs. 5–8). It represents an end-member regarding the strong correlation between Fe and Mn, reaching the highest Fe and Mn concentrations obtained along both epicontinental settings (Fig. 8B and Table 2). Further enhancement of the geochemical differentiation results from the obtained depleted $\delta^{13}C$ ratios (−2.2‰; Table 2), only reflected by these facies with higher siliciclastic content (cluster I; Fig. 7A,B). To account for this geochemical signature, a combination of two probable mechanisms is envisaged: (i) input of ^{12}C from remineralized organic carbon that may lower the $\delta^{13}C$ values as much as 4.0‰ (Immenhauser et al., 2002, 2008), which reinforces primary effects of higher input of nutrients and organic matter levels forcing a strong palaeoenvironmental/palaeoecologic signal in response to such a fertilization increase; and (ii) high porosity and grain size throughout this siliciclastic interval favours meteoric (phreatic) diagenetic imprint (Allan and Matthews, 1982; Lohmann, 1988), as previously discussed for diagenetic influence of this siliciclastic facies on the O-isotope record.

Cluster I therefore represents the maximum continental influence recorded at the compared epicontinental intervals of both settings. Furthermore, it records the maximum diagenetic influence depicted throughout all obtained clusters, combining maximum palaeoenvironmental difference with maximum diagenetic imprint. These particularities make it possible to establish adequate terms of comparison for the remaining clusters.

5.2. Cluster II: spongiolitic buildups

The fully established sponge bioherms at Rocha Poço determine a marked eco-sedimentary, lithostratigraphic (Fig. 2) and geochemical change (cluster II in Fig. 5). The characteristically higher Mg and Sr concentrations are major distinctive features. This interval is related to profound changes in environmental and ecological conditions. On the one hand, higher Mg contents account for a higher relative carbonate content of the sediments throughout this interval (Fig. 5C), in agreement with a local decrease in terrigenous input (Figs. 6 and 8B). All this fits with conditions of comparatively raised bottoms (tectonic readjustment) in response to local tectono-eustatic counteracting of expected effects of the global, second order sea-level rise (Haq et al., 1988; Hardenbol et al., 1998). Hence, carbonate margin progradation, and a related siliciclastic decrease, favoured local sponge growth where mesotrophic conditions were established. The impact on the Mg content of alternative mineralogy changes (high- *vs.* low-magnesium calcite), and/or changes in seawater temperature, are hard to ascertain as these may potentially be superimposed by the clearly identified increase in carbonate content (Figs. 5, 6 and 8).

Further support for the particularity of the lowermost portion of the spongiolithic limestones (cluster II) was previously presented in

Coimbra et al. (2015) in terms of the geochemical signal of fine detrital carbonate material in-filling interstitial space in sponge buildups (similar to Fig. 3B). These showed lowered $\delta^{13}C$ values with respect to the sponge frame, but such a difference is lost further up-section, when sponge-buildup activity diminished (clusters III and IV at Rocha Poço; Fig. 5).

On the other hand, Sr content is atypically high, reaching the highest values obtained for all clusters (ca. 600 ppm; Table 2 and Fig. 8B). The Rocha Poço area was located at the vicinity of sectors experiencing active reefal-growth under oligotrophic conditions at the Eastern Algarve shelf (Marques, 1985; Ramalho, 1985; Rosendhal, 1985; Leinfelder, 1993). Corals, stromatoporoid-like organisms and algae are the highest accumulators and discriminators for Sr among marine invertebrates (e.g., Bowen, 1956). Reefal patches containing corals and algae (high-level Sr-reservoirs and donors) may have become affected in terms of ecologically favourable/unfavourable conditions by the described relative sea-level dynamics (section 1 and 2). Early diagenetic stabilization and/or dissolution of aragonite thus provided abundant Sr supply to surrounding seawaters, as recorded in cluster II (Coimbra et al., 2015 for details). All of this shows a case of local gradient of nutrients.

5.3. Clusters III and IV: demise of sponge bioherms and hemipelagic rhythmite deposition

One of the most noteworthy findings was that two very well-differentiated lithofacies recorded comparable geochemical trends obtained from the carbonate fraction (Figs. 5–8). The upper spongiolithic interval at Rocha Poço, just above the spongiolithic climax (cluster II), shows no significant geochemical deviation with respect to the Puerto Lorente rhythmite, both thus included in clusters III and IV. This fact allows two readings: (i) either depositional conditions related to the fading-out of the spongiolithic buildup climax at Rocha Poço were not so different from those promoting rhythmite deposition at Puerto Lorente; and/or (ii) potential original geochemical differences were not recorded/analysed, or were homogenized at a rather early diagenetic stage.

For the first alternative (i), relative paleoenvironmental differences only affected the geochemical indicators considered here to a moderate extent. The mesotrophic conditions that favoured the full development of sponge-bioherms during the interval represented by cluster II were probably not persistent throughout Hypselocyclum-Divisum times. Accordingly, nutrient supply for sponge growth was progressively cancelled, accounting for the demise of biogenic build-ups. Low relative sea-levels (Fig. 8B) and unfavourable bottom physiography for upwelling persistence (smoothed seabed relief) may indirectly account for degradation of optimal ecological conditions (nutrient levels) in which sponges thrived. In fact, a third order peak-transgression during the late Divisum Chron favoured a short-time ammonite re-colonization, resulting in a marker limestone bed within the upper spongiolithic facies (ecostratigraphic event in Fig. 3 of Olóriz, 2000; Figs. 2B and 8B).

The overall conditions described for Rocha Poço may not differ significantly from those established at the more uniform, homoclinal ramp, at Puerto Lorente in broad terms of depositional conditions. The latter refer to settings receiving bioclasts from surrounding, raised bottoms colonized by shelly benthics, despite recognized differences in shelf configuration. Thus, far from optimal conditions for sponge buildups, the ecological difference in source areas determined, at most, the accumulation of diverse dominant skeletals in the depositional sites at Rocha Poço and Puerto Lorente. These two settings represent epicontinental areas within the same latitudinal belt, with Rocha Poço being placed slightly landward under the limited influence of detrital material related to a nearby coral-reef fringe. Hence, no major geochemical difference was registered in carbonate matrices, at least concerning the isotopic and elemental signals investigated (Figs. 6–8). The latter alternative (ii) would first imply that other geochemical/mineralogical proxies and complementary sampling of non-carbonate horizons could be necessary to obtain stronger differentiation between the two settings under focus. Yet concerning the variables under scope here, early diagenetic homogenization would be a reasonable assumption for the investigated carbonates, while always subtle enough to preserve nearly the original signature of $\delta^{18}O$ values (Fig. 6B).

A closer look at the differences between clusters III and IV (Fig. 8 and Table 2) reveals that they establish two clear stratigraphic intervals along the Puerto Lorente section, but not in Rocha Poço (Figs. 5C and 8B). Despite a negligible difference in elemental values between the two settings under scope (Table 2 and Fig. 8), a smaller thickness (ca. 20 m vs. 80 m) and a lower number of samples (7 samples vs. 76 samples) make general interpretations at Rocha Poço rather inconclusive. At Puerto Lorente, clusters III and IV do not show strong changes in absolute elemental values (Table 2). For example, the established difference of ca. 500 ppm for Fe concentration or only 11 ppm in Mn abundance between the two clusters can be considered minimal (Table 2). But this subtle trend may be associated with a more expressive 407 ppm variation of Mg, the latter reflecting higher carbonate content (Ca abundance difference of ca. 10,000 ppm; see Table 2). This is in complete agreement with relative sea-level trend (shallowing), with a more arid local climate and consequent lowering of terrigenous input along the upper portion of the Puerto Lorente section (Fig. 8A). All the above means that the performed cluster analysis proves to be a valuable fine-resolution tool for detecting minor, but meaningful palaeoenvironmental geochemical trends.

Apart from the described major trends, prominent Fe and Mn concentration peaks appear along the Puerto Lorente section (Fig. 8A). This feature is noteworthy as it occurs at samples with high carbonate content (>ca. 90%, Fig. 5C), validating the presence of the elements here under scope as carbonate-bound (see also Fig. 8). They reflect major events of terrigenous input, as reflected by the stratigraphic log of this section (base and mid-portion; Fig. 8A). When these events are compared to the 3rd order relative sea-level curve (Fig. 8), the first pulse corresponds to a comparatively high sea-level, while the second one relates to the lowest sea-level envisaged for the studied interval. Hence, when the lowermost siliciclastic peak in Puerto Lorente is compared to the coeval hydrothermal Mn peak at the base of the Rocha Poço section, both can be attributed to tectonic instability along the shelf-system under scope. This is evidence for the differential expression of local to regional tectonic events along the epicontinental fringe, either by increased terrigenous influx (at Puerto Lorente) or affecting ambient seawater geochemistry (at Rocha Poço). This interpretation agrees with clay mineralogy data from the same section (López-Galindo et al., 1991) as well as with widespread regional observations across Iberia and North Africa (Marques et al., 1989, 1991), which can be correlated with a tectonic phase (plate readjustments) encompassing marginal areas related to the evolution of the central North Atlantic Basin (Olóriz et al., 2003).

The recorded Mg concentration trend along the Puerto Lorente section shows some particular features (Fig. 8A). The value of ca. 4000 ppm at the base of this section is followed by a significant decrease down to 2500 ppm, then a progressive recovery back to 4000 ppm along the mixed carbonate-siliciclastic rhythmite. The Mg signature of about 4000 ppm is also reflected by the sedimentary package preceding the stratigraphic interval here under scope, i.e., below the siliciclastic interval. Thus, two aspects need to

be clarified: the higher Mg signature in this epicontinental setting when compared to the very stable signal of 3000 ppm for coeval epioceanic Ammonitico Rosso facies (Coimbra et al., 2015); and the sharp decrease recorded above the siliciclastic interval followed by the slowly recovery trend up-section (Fig. 8A).

Mg concentration in marine carbonates is known to respond to changes in seawater temperature and pCO_2 (Burton and Walter, 1991; Adabi, 2004). The effects of seawater pH, alkalinity, impact on sulphate reduction processes, controls exerted by biologic processes; and/or local current patterns, fall beyond the scope of this contribution. But both temperature and pCO_2 need to be taken into account for the particular setting under focus. Compared with epioceanic records, a slightly warmer water temperature is envisaged for the epicontinental Puerto Lorente section (Fig. 6B), as interpreted from lowered O-isotope values, explaining also the recorded increase in Mg concentration.

The significant decrease and slow recovery towards these higher values (4000 ppm) occurs just after a major tectonic readjustment at the regional scale (e.g., Acosta, 1989; Marques et al., 1989, 1991; López-Galindo et al., 1991; Olóriz et al., 2003), as recognized by the conspicuous siliciclastic interval at the bottom of this section (Fig. 8A). It is here proposed that such a relevant event could release CO_2 into ambient seawater, potentially forcing the obtained lowered Mg values (ca. 2500 ppm). Such tectonic activity could also promote a local increase of seawater temperature due to increased CO_2 levels, potentially counteracting the effect of lowering Mg content (Burton and Walter, 1991). The Mg stratigraphic trend registered throughout the Lower Kimmeridgian shows recovery to standard values for the Puerto Lorente area, accompanying a change towards locally more arid climatic conditions leading to lowered siliciclastic input and consequently increased carbonate deposition on this epicontinental area (lower cluster IV beds; Fig. 8A). Manganese and Fe trends support this interpretation (Figs. 6 and 8A), as well as the decreasing O-isotope values (Fig. 6B).

6. Conclusions

The obtained chemostratigraphic record from carbonate horizons relates to distinctive characteristics of two Kimmeridgian shallow-marine, epicontinental settings characterized by dissimilar platform morphology, degree of connectivity to oceanic waters, circulation patterns, terrigenous input, lithofacies and stratal patterns. Cluster analysis of geochemical data—retrieved from these mid-shelf carbonate records—reveals major elemental trends differentiating shallow marine waters submitted to different degrees of connection with open sea, epioceanic Tethyan waters. Accentuated diagenetic imprint mostly relates to meteoric/phreatic diagenesis affecting the siliciclastic interval, associated with the comparatively landward setting (the Rocha Poço vs. the Puerto Lorente section). The integration of paleoceanographic knowledge with geochemical, geological and palaeoenvironmental information has led to the following inferences:

(i) Continental influence was revealed by the strong Fe and Mn correlation evidenced at both nearshore sites, more marked at the locally rimmed shelf of Rocha Poço, but also detected along the comparatively homogeneous, mixed carbonate-fine-siliciclastic rhythmic deposition on the non-rimmed shelf at Puerto Lorente;

(ii) The obtained signature for biogenic buildups at Rocha Poço is attributed to changes in ecological conditions forced by local upwelling (fertilization) and the influence of coral-fringe effects, thus revealing a case of variable local gradient in nutrient levels;

(iii) Major events of palaeogeographic restructuring were variably recorded along the investigated north-Tethyan epicontinental fringe, either by sudden increases in siliciclastics related to widespread, regional tectonic pulses (bottom instability, changing subsidence) or detected by geochemical deviations (decoupling of Mn and Fe trends);

(iv) A considerably stable background signal of Mg concentration related to warmer seawater conditions along shallow-marine, nearshore/coastal settings, was identified and corroborated by lowered O-isotope values. Strong disruptions of the recorded steady increasing Mg values could be linked to the influence of geochemically altered water-masses due to tectonic activity;

(v) The geochemical approach to characterize packages of carbonate horizons enabled to differentiate shallow-water settings, providing enough sensitivity and reliability to detect palaeoenvironmental differences occurring along different segments of the northwestern Tethyan margin, covering processes ranging from tectonics to relative sea-level dynamics and forced ecology. The presented outcomes are encouraging, and can be seen as a step-forward towards a deeper understanding of the palaeoenvironmental significance of a wide range of elemental and isotopic signals.

Acknowledgements

The authors wish to thank Dieter Buhl, Andrea Niedermayr, Beate Gehnen and Kathrin Schauerte (Ruhr-University Bochum-RUB) for their support during laboratory measurements, and Alberto Montes (University of Granada-UGR) for the preparation of thin sections. J. Sanders is thanked for the English revision. This research was supported by Projects CGL2008-05251-E and CGL2012-39835 (MINECO) and the Research Group RNM-178, Junta de Andalucía, Spain. R. Coimbra is currently supported by the Post-Doctoral Fellowship SFRH/BPD/92376/2013 (Fundação para a Ciência e a Tecnologia, Portugal) and the research units GeoBiotec - UID/GEO/04035/2013 and MARE- UID/MAR/04292/2013.

References

Acosta, P., 1989. Estudio del Jurásico de un sector de la Sierra de Cazorla (Zona Prebética). Bachelor Thesis. Universidad de Granada, Granada, Spain (in Spanish).

Adabi, M., 2004. A re-evaluation of aragonite versus calcite seas. Carbonate Evaporite 19 (2), 133–141.

Allan, J.R., Matthews, R.K., 1982. Isotope signatures associated with early meteoric diagenesis. Sedimentology 29 (6), 797–817.

Andrieu, S., Brigaud, B., Barbarand, J., Lasseur, E., 2017. The complex diagenetic history of discontinuities in shallow-marine carbonate rocks: new insights from high-resolution ion microprobe investigation of $\delta^{18}O$ and $\delta^{13}C$ of early cements. Sedimentology 65 (2), 360–399. https://doi.org/10.1111/sed.12384.

Aquilina, A., Homoky, W.B., Hawkes, J.A., Lyons, T.W., Mills, R.A., 2014. Hydrothermal sediments are a source of water column Fe and Mn in the Bransfield Strait, Antarctica. Geochimica et Cosmochimica Acta 137, 64–80.

Aurell, M., Meléndez, G., Bádenas, B., 2002. East Iberian basins. In: Aurell, C.M., Meléndez, M., Olóriz, F. (Eds.), The Geology of Spain, Geol. Soc. London, edited by W. Gibbons and T. Moreno, Chapter 11- The Jurassic, pp. 223–235. London, UK.

Azéma, J., Foucault, A., Fourcade, E., García-Hernández, M., González-Donoso, J.M., Linares, D., López-Garrido, A.C., Rivas, P., Vera, J.A., 1979. Las microfacies del Jurásico y Cretácico de las Zonas Externas de las Cordilleras Béticas. Secraría de Publicaciones de la Universidad de Granada, p. 83 (in Portuguese).

Bennett, S.A., Achterberg, E.P., Connelly, D.P., Statham, P.J., Fones, G.R., German, C.R., 2008. The distribution and stabilisation of dissolved Fe in deep-sea hydrothermal plumes. Earth and Planetary Science Letters 270, 157–167.

Bowen, H.J.M., 1956. Strontium and Barium in sea water and marine organisms. Journal of the Marine Biological Association of the United Kingdom 35, 451–460.

Brand, U., Veizer, J., 1980. Chemical diagenesis of a multicomponent carbonate system - 1: trace elements. Journal of Sedimentary Research 50 (4), 1219–1236.

Burton, E.A., Walter, L.M., 1991. The effects of pCO_2 and temperature on magnesium incorporation in calcite in seawater and $MgCl_2$-$CaCl_2$ solutions. Geochimica et Cosmochimica Acta 55 (3), 777–785.

Caracuel, J.E., Olóriz, F., Sarti, C., 1997. Environmental evolution during the late Jurassic at Lavarone (Trento plateau, Italy). Palaeogeography, Palaeoclimatology, Palaeoecology I 35, 163–177.
Christ, N., Immenhauser, A., Amour, F., Mutti, M., Preston, R., Whitaker, F.F., Peterhänsel, A., Egenhoff, S.O., Dunn, P.A., Agar, S.M., 2012. Triassic Latemar cycle tops - Subaerial exposure of platform carbonates under tropical arid climate. Sedimentary Geology 265-266, 1–29.
Cohen, K.M., Finney, S.C., Gibbard, P.L., Fan, J.-X., 2013. The ICS international chronostratigraphic chart. Episodes 36, 199–204. Chart Drafted by K.M. Cohen, D.A.T. Harper, P.L. Gibbard (c) International Commission on stratigraphy, February 2017 - v 2017/2.
Coimbra, R., Olóriz, F., 2012a. Geochemical evidence for sediment provenance in mudstones and fossil-poor wackestones (Upper Jurassic, Majorca Island). Terra Nova 24, 437–445.
Coimbra, R., Olóriz, F., 2012b. Contrast comparison of differential diagenetic pathways of Lower Tithonian carbonate materials from the Betic Cordillera (S Spain): evidence for physico-chemical palaeo-seawater properties. Palaeogeography, Palaeoclimatology, Palaeoecology 321–322, 65–79.
Coimbra, R., Immenhauser, A., Olóriz, F., 2009. Matrix micrite $\delta^{13}C$ and $\delta^{18}O$ reveals synsedimentary marine lithification in upper Jurassic Ammonitico Rosso limestones (betic Cordillera, SE Spain). Sedimentary Geology 219, 332–348.
Coimbra, R., Immenhauser, A., Olóriz, F., 2014. Spatial geochemistry of Upper Jurassic marine carbonates (Iberian subplate). Earth-Science Reviews 139, 1–32.
Coimbra, R., Immenhauser, A., Olóriz, F., Rodríguez-Galiano, V., Chica-Olmo, M., 2015. New insights into geochemical behaviour in ancient marine carbonates (Upper Jurassic Ammonitico Rosso): novel proxies for interpreting sea-level dynamics and palaeoceanography. Sedimentology 62 (1), 266–302.
Coimbra, R., Olóriz, F., 2012. Pixel counting for percentage estimation: applications to sedimentary petrology. Computers & Geosciences 42, 212–216.
Coimbra, R., Azerêdo, A.C., Cabral, M.C., Immenhauser, A., 2016. Palaeoenvironmental analysis of mid-Cretaceous coastal lagoonal deposits (Lusitanian Basin, W Portugal). Palaeogeography, Palaeoclimatology, Palaeoecology 446, 308–325.
Coimbra, R., Horikx, M., Huck, S., Heimhofer, U., Immenhauser, A., Rocha, F., Dinis, J., Duarte, L.V., 2017. Statistical evaluation of elemental concentrations in shallow-marine deposits (Cretaceous, Lusitanian Basin). Marine and Petroleum Geology 86, 1029–1046.
Colombié, C., Giraud, F., Schnyder, J., Götz, A.E., Boussaha, M., Aurell, M., Bádenas, B., 2014. Timing of sea level, tectonics and climate events during the uppermost Oxfordian (Planula Zone) on the Iberian ramp (northeast Spain). Palaeogeography, Palaeoclimatology, Palaeoecology 412, 17–31.
Corbin, J.C., Person, A., Iatzoura, A., Ferre, B., Renard, M., 2000. Manganese in pelagic carbonates: indication of major Tectonic events during the geodynamic evolution of a passive continental margin (the Jurassic European margin of the Tethys-Ligurian Sea). Palaeogeography, Palaeoclimatology, Palaeoecology 156 (1–2), 123–138.
Costa, E.S., Grilo, C.F., Wolff, G.A., Thompson, A., Figueira, R.C.L., Sá, F., Neto, R.R., 2016. Geochemical records in sediments of a tropical estuary (Southeastern coast of Brazil). Regional Studies in Marine Science 6, 49–61.
Elrod, V.A., Berelson, W.M., Coale, K.H., Johnson, K.S.C.L., 2004. The flux of iron from continental shelf sediments: a missing source for global budgets. Geophysical Research Letters 31 (12), L12307. https://doi.org/10.1029/2004GL020216.
Feely, R.A., Massoth, G.J., Baker, E.T., Lebon, G.T., Geiselman, T.L., 1992. Tracking the dispersal of hydrothermal plumes from the Juan de Fuca Ridge using suspended matter compositions. Journal of Geophysical Research Solid Earth 97 (B3), 3457–3468.
García-Hernández, M., López- Garrido, A.C., Rivas, P., Sanz de Galdeano, C., Vera, J.A., 1980. Mesozoic palaeogeographic evolution of the external zones of the betic Cordillera. Geologica Mijnbouw 59, 155–168.
Godet, A., Durlet, C., Spangenberg, J.E., Fölmi, K.B., 2016. Estimating the impact of early diagenesis on isotope records in shallow-marine carbonates: a case study from the Urgonian Platform in western Swiss Jura. Palaeogeography, Palaeoclimatology, Palaeoecology 454, 125–138.
Haq, B.U., Hardenbol, J., Vail, P.R., 1987. Chronology of fluctuating sea levels since the Triassic (250 million years ago to present). Science 235, 1156–1167.
Haq, B.U., Hardenbol, J., Vail, P., 1988. Mesozoic and Cenozoic chronostratigraphy and cycles of sea-level change. In: Wilgus, C., et al. (Eds.), Sea-level Change: An Integrated Approach, vol. 42. SEPM Special Publication, pp. 71–108.
Hardenbol, J., Thierry, J., Farley, M.B., Jacquin, T., DeGraciansky, P.-C., Vail, P.R., 1998. Mesozoic-Cenozoic sequence chronostratigraphic framework. In: DeGraciansky, P.-C., et al. (Eds.), Sequence Stratigraphy of European Basins, SEPM Special Publication 60, Charts, pp. 3–13.
Huck, S., Wohlwend, S., Coimbra, R., Christ, N., Weissert, H., 2017. Disentangling shallow-water bulk carbonate carbon isotope archives with evidence for multi-stage diagenesis: an in-depth component specific petrographic and geochemical study from Oman (mid-Cretaceous). The Depositional Record. https://doi.org/10.1002/dep2.35.
Immenhauser, A., Holmden, C., Patterson, W.P., 2008. Interpreting the carbon-isotope record of ancient shallow epeiric seas: Lessons from the recent. In: Pratt, B.R., Holmden, C. (Eds.), Dynamics of Epeiric Seas. Geological Association of Canada Special Publication, pp. 135–174.
Immenhauser, A., Kenter, J.A.M., Ganssen, G., Bahamonde, J.R., van Vliet, A., Saher, M.H., 2002. Origin and significance of isotope shifts in Pennsylvanian carbonates (Asturias, NW Spain). Journal of Sedimentary Research 72 (1), 82–94.
Kickmaier, W., Peters, T., 1990. Manganese occurrences in the Al Hamah range Wahrah formation, Oman mountains. In: Robertson, A.H.F., Searle, M.P., Ries, A.C. (Eds.), The Geology and Tectonics of the Oman Region, vol. 49. Geological Society of London Special Publication, pp. 239–249.
Klinkhammer, G., Hudson, A., 1986. Dispersal patterns for hydrothermal plumes in the South Pacific using manganese as a tracer. Earth and Planetary Science Letters 79 (3), 241–249.
Lécuyer, Ch., Picard, St., Garcia, J.-P., Sheppard, S.M.F., Grandjean, P., Dromart, G., 2003. Thermal evolution of Tethyan surface waters during the Middle-Late Jurassic: evidence from $\delta^{18}O$ values of marine fish teeth. Palaeoceanography 18 (3), 21.1–21.16.
Leinfelder, R., 1993. Upper Jurassic reef types and controlling factors. A preliminary report. Profil 5, 1–45.
Lohmann, K.C., 1988. In: James, N.P., Choquette, P.W. (Eds.), Geochemical Patterns of Meteoric Diagenetic Systems and Their Application to Studies of Palaeokarst, in Palaeokarst. Springer Verlag, Berlin, pp. 58–80.
López-Galindo, A., Olóriz, F., Rodríguez-Tovar, F.J., 1991. Mineralogical analysis in marly intercalations and integrated approaches to palaeoenvironmental interpretation. An example from the South Iberian margin during the Upper Jurassic: 7th Euroclay Conference. In: Proceedings, vol. 2, pp. 707–712.
López-Galindo, A., Olóriz, F., Rodriguez-Tovar, F.J., 1994. Geochemical traces and sequence stratigraphy analysis during the upper Jurassic in Southern Iberia. Mineralogical Magazine 58A, 531–532.
Lupton, J.E., Craig, H., 1981. A major helium-3 source at 15°S on the east Pacific rise. Science 214 (4516), 13–18.
Mannupella, G., Marques, B., Rocha, R., 1988. Evolution tectono-sedimentaire du Bassin de l'Algarve pendant le Jurassique. In: Rocha, R.B., Soares, A.F. (Eds.), 2nd International Symposium of Jurassic Stratigraphy, pp. 1031–1046. Lisbon, Portugal.
Marques, B., 1983. Oxfordiano-Kimeridgiano do Algarve Oriental: estratigrafia, palaeobiologia (Ammonoidea) e palaeobiogeografia. PhD thesis. Univ. Nova Lisboa, Lisbon, Portugal.
Marques, B., 1985. Litostratigrafia do Oxfordiano-Kimmeridgiano do Algarve. Comunicações dos Serviços Geológicos de Portugal 71, 33–39 (in Portuguese).
Marques, B., Olóriz, F., 1989a. La marge Sud-Ouest d'Iberie pendant le Jurassique superieur (Oxfordien-Kimmeridgien): essai de reconstruction geo-biologique. Cuadernos de Geología Ibérica 13, 251–263 (in Portuguese).
Marques, B., Olóriz, F., 1989b. La plate-forme de 1'Algarve au Jurassique supérieur: les grandes discontinuites stratigraphiques. Cuadernos de Geología Ibérica 13, 237–249 (in Portuguese).
Marques, B., Olóriz, F., Rodriguez-Tovar, F.J., 1989. Interactions between tectonics and eustatism. Examples from the south or Iberia. Strata 5, 119–120.
Marques, B., Olóriz, F., Rodriguez-Tovar, F.J., 1991. Interactions between tectonics and eustasy during the upper Jurassic and lowermost cretaceous. Examples from the south of Iberia. Bulletin de la Société Géologique de France 162 (6), 1109–1124.
Marques, B., Olóriz, F., 1992. The Orthaspidoceras uhlandi (OPPEL) record and the maximum flooding in the eastern Algarve during the lower Kimmeridgian. Revista Española de Palaeontologia, extra 3, 149–156.
Marshall, J.D., 1992. Climatic and oceanographic isotopic signals from the carbonate rock record and their preservation. Geological Magazine 129 (2), 143–160.
McCrea, J.M., 1950. On the isotopic chemistry of carbonates and a paleotemperature scale. Journal of Chemical Physics 18, 849–857.
Middag, R., de Baar, H.J.W., Laan, P., Klunder, M.B., 2011. Fluvial and hydrothermal input of manganese into the Arctic Ocean. Geochimica et Cosmochimica Acta 75 (9), 2393–2408.
Ogg, J.G., Ogg, G.M., Gradstein, F.M., 2016. A Concise Geologic Time Scale. Elsevier, p. 234.
Olóriz, F., 2000. Time-averaging and long-term palaeoecology in macroinvertebrate fossil assemblages with ammonites (Upper Jurassic). Revue Paléobiologie, Geneve, Volume Spécial 8, 123–140.
Olóriz, F., 2002. In: Aurell, C.M., Meléndez, M., Olóriz, F. (Eds.), Betic Cordillera, in the geology of Spain, edited by W. Gibbons and T. Moreno, Chapter 11–The Jurassic. Geological Society of London, London, UK, pp. 235–237.
Olóriz, F., Rodríguez-Tovar, F.J., 1993. Lower Kimmeridgian biostratigraphy in the central Prebetic (southern Spain. Cazorla and Segura de la Sierra sectors). Neues Jahrbuch für Geologie und Palaontologie 3, 150–170.
Olóriz, F., Rodríguez-Tovar, F.J., 2000. Diplocraterion: a useful marker for sequence stratigraphy and correlation in the Kimmeridgian, Jurassic (Prebetic zone, betic Cordillera, southern Spain). Palaios 15, 546–552.
Olóriz, F., Rodríguez-Tovar, F.J., Chica-Olmo, M., Pardo, E., 1992. The marl-limestone rhythmites from the Lower Kimmeridgian (Platynota Zone) of the central Prebetic and their relationship with variations in orbital parameters. Earth-Science Reviews 111, 407–424.
Olóriz, F., Rodríguez-Tovar, F.J., 1998. Multifactorial control on deposition of epicontinental hemipelagic carbonates during the earliest Kimmeridgian (Prebetic Zone, southern Spain). Sedimentary Geology 119, 123–139.
Olóriz, F., Rodríguez-Tovar, F.J., 1999. Análisis palaeoicnológico del perfil de Puerto Lorente (Kimmeridgiense, Sierra de Cazorla, Prebético Externo), Revista Española de Palaeontología, n° extra Homenaje al Prof. J. Truyols, 15–28 (in Spanish).
Olóriz, F., Marques, B., Rodriguez-Tovar, F.J., 1991. Eustatism and faunal associations. Examples from the southern Iberian margin during the late Jurassic (Oxfordian-Kimmeridgian). Eclogae Geologiae Helvetiae 84 (1), 83–106 (in Spanish).

Olóriz, F., Marques, B., Moliner, L., 1988. The platform effect: an example from Iberian shelf areas in the lowermost Kimmeridgian. In: 2nd International Symposium on Jurassic Stratigraphy, Lisbon, vol. 2, pp. 534–562.

Olóriz, F., Rodriguez-Tovar, F.J., Marques, B., Caracuel, J.E., 1993. Ecostratigraphy and sequence stratigraphy in the high frequency sea-level fluctuations: example from Jurassic macroinvertebrate assemblages. Palaeogeography, Palaeoclimatology, Palaeaecology 101, 131–145.

Olóriz, F., Rodríguez-Tovar, F.J., Marques, B., 1994. Macroinvertebrate assemblages and ecostratigraphic structuration within a highstand system Tract. An example from the lower Kimmeridgian in southern Iberia. Geobios M.S. 17, 605–614.

Olóriz, F., Villaseñor, F., González-Arreola, C., 2003. Major lithostratigraphic units in land-outcrops in north-central Mexico and the subsurface of the northern rim of the Gulf of Mexico Basin (Upper Jurassic–lowermost Cretaceous): a proposal for correlation of tectono-eustatic sequences. Journal of South American Earth Sciences 16 (3), 119–142.

Parente, M., Frijia, G., Di Lucia, M., 2007. Carbon-isotope stratigraphy of Cenomanian-Turonian platform carbonates from the southern Apennines (Italy): a chemostratigraphic approach to the problem of correlation between shallow-water and deep-water successions. Journal of the Geological Society 164, 609–620.

Pendas, F., 1971. Definición morfológica de los embalses subterráneos del alto sureste español. In: I Congreso Hispano-Luso-Americano de Geología Económica, Sección Hidrogeología, II, pp. 529–550 (in Spanish).

Price, G.D., Sellwood, B.W., 1994. Palaeotemperature indicated by upper Jurassic (Kimmeridgian Tithonian) fossils from Mallorca determined by oxygen-isotope composition. Palaeogeography, Palaeoclimatology, Palaeaecology 110, 1–10.

Ramalho, M., 1985. Considerations sur la biostratigraphie de Jurassique Supérieur de l' Algarve Oriental (Portugal). Comunicações dos Serviços Geológicos de Portugal 71, 41–50 (in Portuguese).

Ramalho, M., 1988. Sur la découverte de biohermes stromatolithiques à spongiaires siliceux dans le Kimméridgien de l'Algarve, Portugal. Comunicações dos Serviços Geológicos de Portugal 74, 41–55 (in Portuguese).

Rosendhal, S., 1985. Die oberjurassische Korallenfazies von Algarve (Südportugal). Arbeiten aus dem Institut für Geologie und Paläontologie der Universität Stuttgart, Neue Folge, pp. 82–125 (in Portuguese).

Rubin, K., 1997. Degassing of metals and metalloids from erupting seamount and mid-ocean ridge volcanoes: observations and predictions. Geochimica et Cosmochimica Acta 61 (17), 3525–3542.

Sellwood, B.W., Valdes, P.J., 2006. Mesozoic climates: general circulation models and the rock record. Sedimentary Geology 190, 269–287.

Sessa, J.A., Ivany, L.C., Schlossnagle, T.H., Samson, S.D., Schellenberg, S.A., 2012. The fidelity of oxygen and strontium isotope values from shallow shelf settings: implications for temperature and age reconstructions. Palaeogeography, Palaeoclimatology, Palaeoecology 342–343, 27–39.

Stampfli, G.M., Borel, G.D., 2002. A plate tectonic model for the Palaeozoic and Mesozoic constrained by dynamic plate boundaries and restored synthetic oceanic isochrons. Earth and Planetary Science Letters 196 (1–2), 17–33.

Thierry, J., Abbate, E., Alekseev, A.S., Ait, O.R., Ait, S.H., Bouaziz, S., Canerot, J., Georgiev, G., Guiraud, R., Hirsch, F., Ivanik, M., Le, M.J., Le, N.Y.M., Medina, F., Mouty, M., Nazarevich, B., Nikishin, A.M., Page, K., Panov, D.L., Pique, A., Poisson, A., Sandulescu, M., Sapunov, I.G., Seghedi, A., Soussi, M., Tchoumatchenko, P.V., Vaslet, D., Vishnevskaya, V., Volozh, Y.A., Voznezenski, A., Walley, C.D., Wong, T.E., Ziegler, M., Barrier, E., Bergerat, F., Bracene, R., Brunet, M.F., Cadet, J.P., Guezou, J.C., Jabaloy, A., Lepvrier, C., Rimmele, G., de, W.P., Baudin, F., Belaid, A., Bonneau, M., Coutelle, A., Fekirine, B., Guillocheau, F., Hantzpergue, M., Julien, M., Kokel, F., Lamarche, J., Mami, L., Mansy, J.L., Mascle, G., Pascal, C., Robin, C., Stephenson, R., Sihamdi, N., Vera, J.A., Vuks, V.J., 2000a. Early Kimmeridgian (146–144 Ma). In: Dercourt, J., Gaetani, M., Vrielynck, B., Barrier, E., Biju Duval, B., Brunet, M.F., Cadet, J.P., Crasquin, S., Sandulescu, M. (Eds.), Peri-Tethys Atlas; Palaeogeographical Maps; Explanatory Notes, Commission for the Geologic Map of the World, Paris, pp. 85–97.

Thierry, J., Abbate, E., Alekseev, A.S., Ait, O.R., Ait, S.H., Bouaziz, S., Canerot, J., Georgiev, G., Guiraud, R., Hirsch, F., Ivanik, M., Le, M.J., Le, N.Y.M., Medina, F., Mouty, M., Nazarevich, B., Nikishin, A.M., Page, K., Panov, D.L., Pique, A., Poisson, A., Sandulescu, M., Sapunov, I.G., Seghedi, A., Soussi, M., Tchoumatchenko, P.V., Vaslet, D., Vishnevskaya, V., Volozh, Y.A., Voznezenski, A., Walley, C.D., Wong, T.E., Ziegler, M., Barrier, E., Bergerat, F., Bracene, R., Brunet, M.F., Cadet, J.P., Guezou, J.C., Jabaloy, A., Lepvrier, C., Rimmele, G., de, W.P., Baudin, F., Belaid, A., Bonneau, M., Coutelle, A., Fekirine, B., Guillocheau, F., Hantzpergue, M., Julien, M., Kokel, F., Lamarche, J., Mami, L., Mansy, J.L., Mascle, G., Pascal, C., Robin, C., Stephenson, R., Sihamdi, N., Vera, J.A., Vuks, V.J., 2000b. Middle Callovian (157–155Ma). In: Dercourt, J., Gaetani, M., Vrielynck, B., Barrier, E., Biju Duval, B., Brunet, M.F., Cadet, J.P., Crasquin, S., Sandulescu, M. (Eds.), Peri-Tethys Atlas; Palaeogeographical Maps; Explanatory Notes, Commission for the Geologic Map of the World, Paris, pp. 85–97.

van der Kooij, B., Immenhauser, A., Csoma, A., Bahamonde, J., Steuber, T., 2009. Spatial geochemistry of a Carboniferous platform-margin-to-basin transect: balancing environmental and diagenetic factors. Sedimentary Geology 219 (1–4), 136–150.

Veizer, J., 1983. Chemical analysis of carbonates: theory and application of trace element technique. In: Stable Isotopes in Sedimentary Geology, SEPM Short Course No. 10. SEPM, Dallas, 3/1-3/100.

Vincent, B., Rambeau, C., Emmanuel, L., Loreau, J.P., 2006. Sedimentology and trace element geochemistry of shallow-marine carbonates: an approach to palaeoenvironmental analysis along the Pagny-sur-Meuse Section (Upper Jurassic, France). Facies 52 (1), 69–84.

Wierzbowski, H., 2004. Carbon and oxygen isotope composition of Oxfordian-Early Kimmeridgian belemnite rostra: palaeoenvironmental implications for Late Jurassic seas. Palaeogeography, Palaeoclimatology, Palaeocology 203, 153–168.

Zhao, M.-Y., Zheng, Y.-F., 2014. Marine carbonate records of terrigenous input into Palaeotethyan seawater: geochemical constraints from Carboniferous limestones. Geochimica et Cosmochimica Acta 141, 508–531.